EUROPEAN COMMISSION
JOINT RESEARCH CENTRE
Environment Institute
Renewable Energies Unit
I-21020 Ispra (VA) Italy

Hydrogen Isotopes Diffusive Transport in Tungsten

G.A. Esteban, A. Perujo, K. Douglas

2000

EUR 19654 EN

EUROPEAN COMMISSION
JOINT RESEARCH CENTRE
Environment Institute
Renewable Energies Unit
I-21020 Ispra (VA) Italy

Hydrogen Isotopes Diffusive Transport in Tungsten

G.A. Esteban, A. Perujo, K. Douglas

2000

EUR 19654 EN

LEGAL NOTICE

EUR 19654 EN

Printed in Italy

HYDROGEN ISOTOPES DIFFUSIVE TRANSPORT IN TUNGSTEN

G. A. Esteban, A. Perujo and K. Douglas

Commission of the European Communities
Joint Research Centre – Ispra Site
Environment Institute, Renewable Energy Unit
21020 Ispra (VA), Italy

ABSTRACT

The time dependent gas-phase isovolumetric desorption technique has been used with protium and deuterium over a temperature range of 673 to 1073 K and driving pressures ranging from $1.3 \cdot 10^4$ to 10^5 Pa, to obtain the hydrogen diffusive transport parameters: diffusivity (D), Sieverts' constant (K_s) and permeability (Φ), and the trapping parameters: the trap site concentration (N_t) and the trapping energy (E_t), in pure tungsten.

For protium, the following parameters have been evaluated:

$D(m^2s^{-1})=5.682 \cdot 10^{-10}\exp(-9278/RT)$,

$K_s(mol\ m^{-3}Pa^{-1/2})=2.896 \cdot 10^{-2}\ \exp(-26879/(RT))$,

$\Phi(mol\ m^{-1}Pa^{-1/2}s^{-1})=1.645 \cdot 10^{-11}\ \exp(-36158/RT)$.

$E_t(J/mol)=86586$,

$N_t(sites/m^3)=2.75\ 10^{23}$.

For deuterium:

$D(m^2s^{-1})=5.490 \cdot 10^{-10}\exp(-9995/RT)$,

$K_s(mol\ m^{-3}Pa^{-1/2})=2.748 \cdot 10^{-2}\ \exp(-28740/RT)$,

$\Phi(mol\ m^{-1}Pa^{-1/2}s^{-1})=1.508 \cdot 10^{-11}\ \exp(-38736/RT)$.

$E_t(J/mol)=93658$,

$N_t(sites/m^3)=1.33\ 10^{23}$.

On the basis of ideal harmonic vibration of the hydrogen isotope atoms in a unique type of solution site, the values derived for the characteristic protium oscillation temperatures are: θ =893 K and θ^*=2467 K. These values lead to the following extrapolated tritium transport parameters:

$D(m^2s^{-1})=5.342\cdot10^{-10}\exp(-11166/RT)$,

$K_s(mol\ m^{-3}Pa^{-1/2})=2.246\cdot10^{-2}\exp(-27751/RT)$,

$P(mol\ m^{-1}Pa^{-1/2}s^{-1})=1.200\cdot10^{-11}\exp(-38917/RT)$.

$E_t(J/mol)=100453$,

$N_t(sites/m^3)=3.22\ 10^{23}$.

SUMMARY

LIST OF TABLES

LIST OF FIGURES

1. INTRODUCTION

Besides carbon and berilium, the high-Z material tungsten has been identified as a suitable candidate to be used as plasma facing material, in the limiters and several parts of the divertor (the divertor dome, the divertor baffle, the transparent wall and the energy dump targets) contained in the ITER concept of a thermonuclear fusion reactor [1, 2].

In addition to excellent thermo-mechanical properties (good thermal conductivity and high temperature strength), tungsten exhibits a good behaviour concerning the exposure of the material to a fusion plasma; i.e., it shows a high energy threshold for physical sputtering, the highest melting point and the lowest vapour pressure of all metals and it does not form hydrides or co-deposits with tritium (H_T). This combination of physical and mechanical properties makes tungsten very attractive for its inclusion in the high heat flux components mentioned above.

The characterisation of the interaction between hydrogen (H) and tungsten is indispensable when quantifying issues of safety, breeding feasibility, fuel economy and plasma stability of a future fusion reactor using this plasma facing material. Moreover, the H transport parameters in tungsten are the factors governing the H_T and deuterium (H_D) inventory and the permeation and recycling of H_T through the high heat flux components using this type of material.

It exists a scarcity of reliable data of H isotope transport in tungsten, probably owing to its slow transport kinematics that makes its experimental measurement strenuous (long measurement times may be required and a certain gauging accuracy must be assured in order to avoid background noise perturbations). Furthermore, the existent data coming from different works [3-7], show an enormous deviation from one another.

In the present work a series of gas/phase isovolumetric desorption experiments (IDE), (Sieverts' apparatus), have been undertaken over a broad range of temperatures, from 673 to 1073 K, and partial pressures ranging from $1.3 \cdot 10^4$ to 10^5 Pa, in order to obtain the H isotopes diffusive transport parameters permeability Φ (mol $m^{-1}s^{-1}Pa^{-1/2}$), diffusivity D (m^2s^{-1}) and Sieverts' constant K_s ($mol \cdot m^{-3}Pa^{-1/2}$). The trapping parameters, the number of trap sites N_t (sites/m^3), and the trapping activation energy, E_t (J/mol), are also evaluated.

2. REVIEW OF EXISTING DATA

Here the principal H diffusive transport parameters in tungsten found in the literature are reviewed. Table 1 shows lattice Sieverts' constant and diffusivity pre-exponentials, K_{s0} and D_0, and their respective activation energies, the solution energy, E_s, and the diffusion energy, E_d. In Table 2 the characteristic trapping parameters: the trap site density, N_t, and the trapping energy, E_t, are tabulated.

The most customary referenced experimental values are those obtained by R. Frauenfelder [3]. In this case a gas evolution method was used with rolled sintered tungsten for a H loading pressure of $8 \cdot 10^4$ Pa and temperatures between 1100 and 2400 K; the H diffusivity and solubility were calculated by modeling the H degassing of a previously loaded specimen. The fundamental background of this technique is the same as the one used in the present work. However, there are some different features to be outlined:

In [3], between loading and release phases the volume containing the sample was continuously pumped-down during a long period of time ("overnight") at room temperature and the H desorbed from the specimen during this pumping period was neglected. The release phase was triggered by a flash heating of the sample that takes some time ("3 minutes") to reach the desired constant temperature level. The H release was studied in continuous pumping conditions; the model assumed a constant pumping speed of a diffusion pump, what is fulfilled provided the operational conditions of the pump are strictly maintained.

Kizu et.al. [4] used the classical gas permeation technique with polycristalline-W membranes manufactured by powder metallurgy. The measurements were performed at the temperature range 783 to 1091 K with H pressure ranging from 10^1 to 10^3 Pa.

Moore and Unterwald [5] studied the atomisation phenomenon, of H molecules, $H_2 \leftrightarrow 2H$, on the hot surface of a tungsten filament in the temperature range 1200 to 2500 K. The discrepancy detected between the molecular inventory diminution and the generated atomic inventory was explained in terms of H absorption and diffusion in the bulk of the W-filament. The transient rates of absorption were modelled raising the characterisation of solubility and diffusion parameters of H in tungsten.

Table 1. Experimental hydrogen Sieverts' constants and diffusivities of tungsten.

Material	K_{s0}(mol $m^{-3}Pa^{-1/2}$)	E_s(kJ mol^{-1})	D_0(m^2s^{-1})	E_d(kJ mol^{-1})	Temperature(K)	Reference
Sintered and rolled cylinder	1.480	101.0	$4.1\cdot10^{-7}$	37.7	1100-2400	[3]
Polycristalline-W membranes	140	22.3	$2.8\cdot10^{-8}$	63.1	783-1091	[4]
Filament ribbon	1039 (at 2713 K)	267.9	$7.2\cdot10^{-8}$	173.75	1510-1902	[5]
Poly&monocristalline-W tubes	$1.22\cdot10^{-4}$	2.9	$6.0\cdot10^{-4}$	103.41	400-1200	[6]
1mm-diameter commercial wire	-	-	$8.1\cdot10^{-6}$	82.89	1055-1570	[7]
Single cristal	-	-	$3\cdot10^{-10}$	24.12	300-800	[8]
Wrought	-	-	$1.5\cdot10^{-10}$	24.12	300-800	

Table 2. Experimental hydrogen trapping parameters of tungsten.

Characteristics	E_t (kJ mol^{-1})	N_t (sites m^{-3})	Reference
- Single crystal (natural traps)	48.2	$3.8\cdot10^{26}$	[8]
(ion induced, 1.5, 8 KeV D^+)	120.6	$1.0\cdot10^{28}$	
- Wrought (natural traps)	48.2	$6.33\cdot10^{26}$	
- Pure W rolled 0.3 mm foil		-	[9]
(weak deffects)	53.0	-	
(ion induced, 1.5, 8 KeV D^+)	96.5	-	
- Polycristalline			[10]
(Unannealed)	150.5	$4.37\cdot10^{24}$	
(Annealed 1273 K)	137.0	$1.65\cdot10^{24}$	
(Annealed 1673 K)	129.3	$8.23\cdot10^{23}$	

Zakharov & Sharapov [6] measured the permeation of H through a tube of tungsten (with a sealed end) from 673 to 1473 K and pressures from $1.3 \cdot 10^2$ to $2.6 \cdot 10^4$ Pa. The tungsten specimen was polycrystalline textured and was manufactured by vapor-gas phase tungsten hexafluoride reduction.

Ryabchikov [7] modeled the H degassing rates of previously up-to-saturation loaded commercial wires, evaluating diffusivities in the temperature range 1055 to 1570 K.

Franzen et.al. [8] modeled the H trapping in and release from previously implanted tungsten specimens. They studied two type of tungsten specimens: single crystal and wrought, in the temperature range 300 to 800 K, obtaining the H diffusivity and characterizing the trapping phenomenon for differentiated natural and ion-induced traps. An analogous work was developed by Pisarev et.al. [9] studying ion implantation of H_D in tungsten from 350 to 750 K; from the thermodesorption peaks analysis two activation energies for trapping were evaluated.

Anderl et.al [10] used the ion driven permeation technique with H_D in polycrystalline tungsten to study H_D transport and trapping phenomenon. They used diverse specimens of the same material (polycrystalline tungsten foils manufactured by powder metallurgy) but with different annealing temperatures before experimental examination. They noticed the effect of the heat treatment, i.e. the microstructure configuration, in the activation energy of trapping.

3. EXPERIMENTAL

3.1. Material

The material studied is pure, unalloyed, undoped, polycrystalline metallic tungsten. The specimens consisted of four cylinders with a 6-mm diameter and 60-mm height. The specimen dimensions were defined in this manner to make feasible the H transport study using the approximation to an infinite-cylinder geometry. The specimens were cut by means of spark eroding from a rod (6-mm diameter) of material. The material contains a minimum of 99.98% W, and does not exceed the limits of impurities indicated in Table 3.

Table 3. Limits of impurities in tungsten.

Impurity	Limit, ppm	Impurity	Limit, ppm	Impurity	Limit, ppm
Ag	<5	Fe	20	O	10
Al	<10	H	<5	P	20
As	<5	K	<5	Pb	<10
Ba	<5	Mg	<5	S	<2
C	15	Mn	<5	Si	<10
Ca	5	Mo	40	Ta	<5
Cd	<1	N	<5	Ti	5
Co	5	Na	5	Zn	<5
Cr	<10	Nb	<5	Zr	<5
Cu	5	Ni	5		

Each batch tested consisted of four specimens to provide a larger signal to noise ratio for the experiments.

The specimens were used as received without any heat treatment. In Figure 1 the polycrystalline microstructure of the material can be observed.

The specimens were cleaned by etching in a 20% solution of potassium hydroxide in order to remove any oxide residue. Subsequently, the surface was mechanically polished and degreased. Finally, the specimens were dried in a vacuum furnace before insertion into the experimental rig. These processes eliminate any impurity left on the surface that might affect the penetration of H into the bulk of the material.

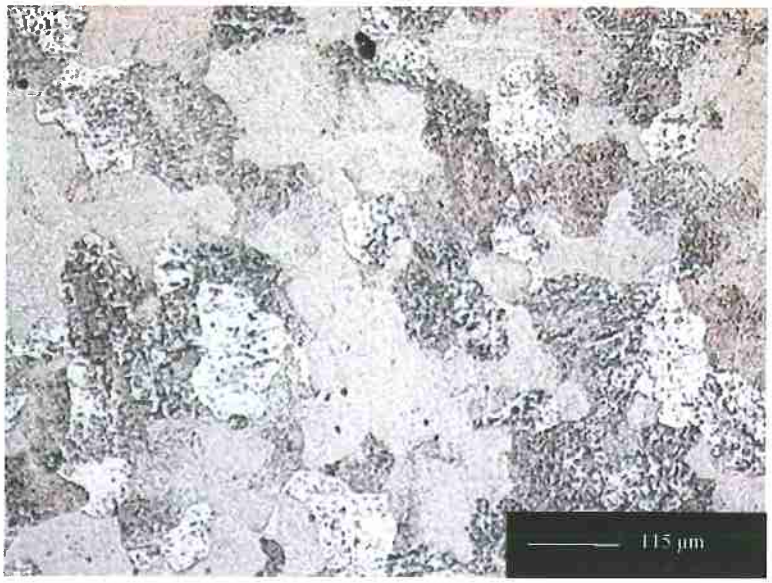

Figure 1. Optical micrograph of Tungsten.

3.2. Experimental rig

A schematic view of the ID installation is shown in Figure 2. This installation and the procedure for a measurement has been described in earlier works [11-14]. The rig comprises ultra high vacuum stainless steel components and volumes in Pyrex glass so that any background H pressure release coming from the outgassing from the walls of the components is minimised. The ultra high vacuum (10^{-7} Pa) is obtained by two pumping units comprising a turbomolecular and a two-stage rotary pump. The specimens are placed into the nozzle of the experimental chamber V1, where a resistance furnace, F, provides the heat needed to operate over the entire range of the measurement temperatures.

Two Pt-resistance thermometers T1 and T2 register the specimen and the experimental chamber temperature, respectively. The evolution of the H pressure in the containing chamber, V1, is gauged by two capacitance manometers, P1, and P2 and a spinning rotor gauge, P4, each one covering certain pressure range from 10^{-5} to 10^{5} Pa. The Quadrupole Mass Spectrometer, QMS, checks the purity of the supplied gas and the gas released from the specimen.

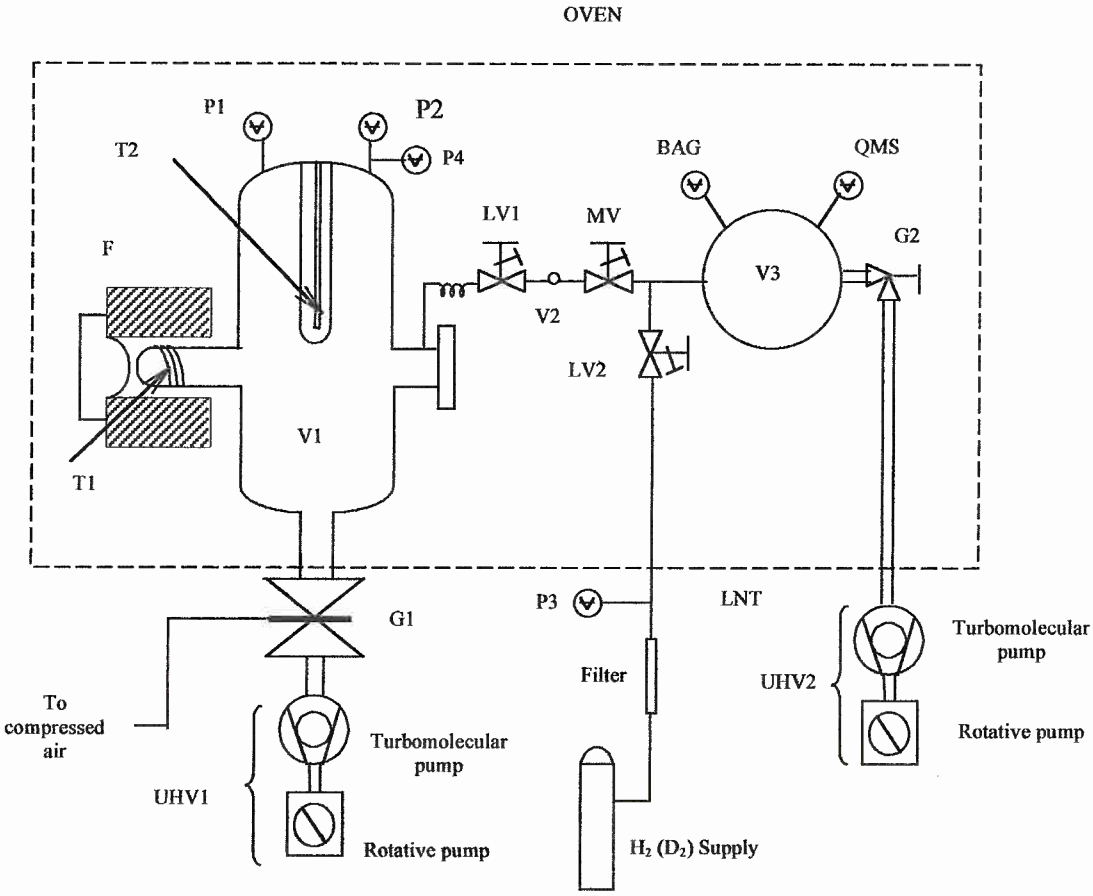

BAG	Bayard-Alpert Gauge	MV	Manually actuated magnetic valve
F	Furnace	P1, P2, P3	Capacitive manometers
G1	Electropneumatic gate valve	P4	Spinning rotor gauge
UHV	Ultra high vacuum pumping units	QMS	Quadrupole mass spectrometer
G2	Manually actuated gate valve	V1	Experimental chamber
T1, T2	Pt-Resistance Thermometers	V2, V3	Expansion volumes
LV1,2	Manually actuated leak valves		

Figure 2. Updated schematic view of the isovolumetric desorption facility.

Some simple modifications have been performed in the rig used here in relation to that used in [11-14]. The gas supplied to the experimental chamber is purified by a zeolite-type filter substituting the previous liquid nitrogen trap. A capacitance manometer P3 has been installed in place of the U-tube mercury manometer to measure the supplied H pressure in order to avoid mercury vapours accompanying the gas. Some valves (LV1 and LV2) had to be substituted to assure perfect vacuum-tightness provoking a change in the Pyrex glass volume of experimental chamber V1; the new effective volume was accurately measured by a series of isothermal expansions of gas into a calibrated volume (Sieverts' method) equalling $5.587 \cdot 10^{-3}$ m^3 instead of the previous volume $5.491 \cdot 10^{-3}$ m^3.

3.3. Experimental procedure

The gas phase IDE method intends, on one hand, to measure the capacity of gas absorption of the material (i.e. solubility described by effective Sieverts' constant, $K_{s,eff}$) and, on the other hand, to assess the kinetics of H migration within the material characterised by the effective diffusivity, D_{eff}.

The material studied, tungsten, exhibits a very low solubility and slow migration kinematics at typical high working temperatures. Because of these properties the H transport is characterised by modelling the gas quantity released from the material that has been previously loaded not necessarily up to saturation, since this action would suppose too long and cost-effective experimental times and stability problems in the gauging devices. Therefore, a single run (Figure 3) consists of recording, for the release period, τ_r, the pressure increase in the vessel V1 due to outgassing from the specimens, which have been previously loaded with H at a given pressure and temperature during a certain period of time, τ_l. During the loading phase the gas concentration in the specimen acquires a certain profile characterised by the H transport constants $K_{s,eff}$ and D_{eff} and the loading time τ_l; this profile is not the plane profile characteristic of a saturation situation (Figure 4). Then, a quick, but thorough, pumping down of the vessel V1 breaks this equilibrium (τ_p), triggering the gas release from the material.

The non-saturation condition in the loading phase requires a non-stationary model to reproduce the H pressure rise during the release phase, wherein too long loading-up-to-saturation times are not required.

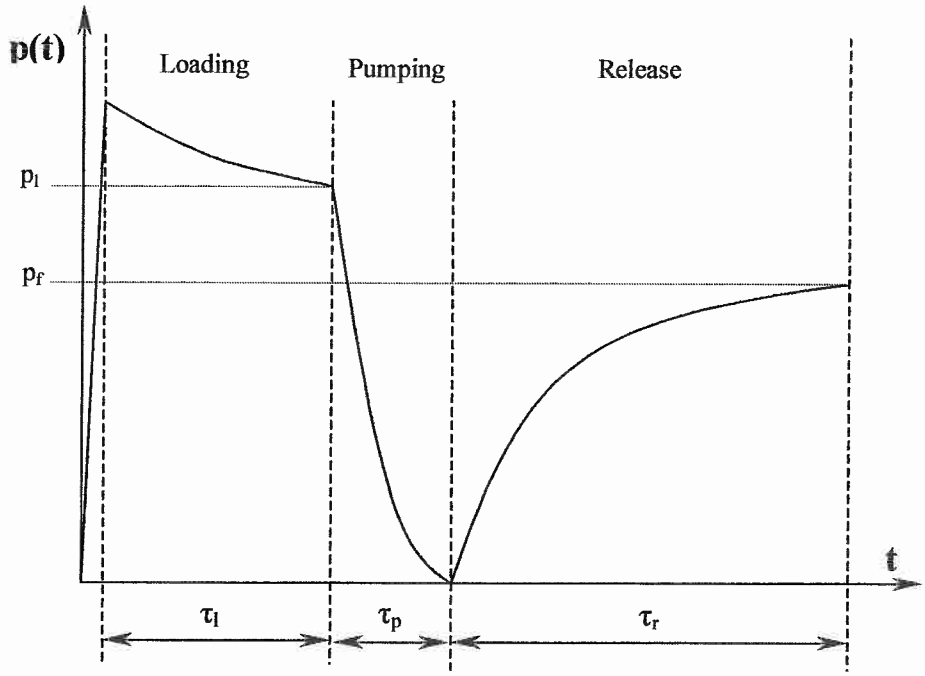

Figure 3. The experimental phases in a single IDE run. The pressure and time scales are different for each phase in order to appreciate their respective pressure profiles. τ_l, τ_p and τ_r are loading pumping and release times respectively, p_l and p_f the pressures measured in the experimental chamber at the end of the loading and release phases, respectively.

This model is developed in the next subsection having in mind that used in [15].

The well calibrated volume of the experimental chamber V1 permits the conversion of the measured pressure increase into an effective amount of released H, or an effective H diffusive flux through the specimen surface at every moment of the desorption phase.

Each measurement is followed by a blank run, under the same experimental conditions, (i.e. same loading pressure, specimens temperature and times τ_l, τ_p, τ_r), without specimens, to account for the contribution of the inner wall outgassing of the vessel V1. The "net" pressure release curve is obtained then by point-to-point pressure subtraction.

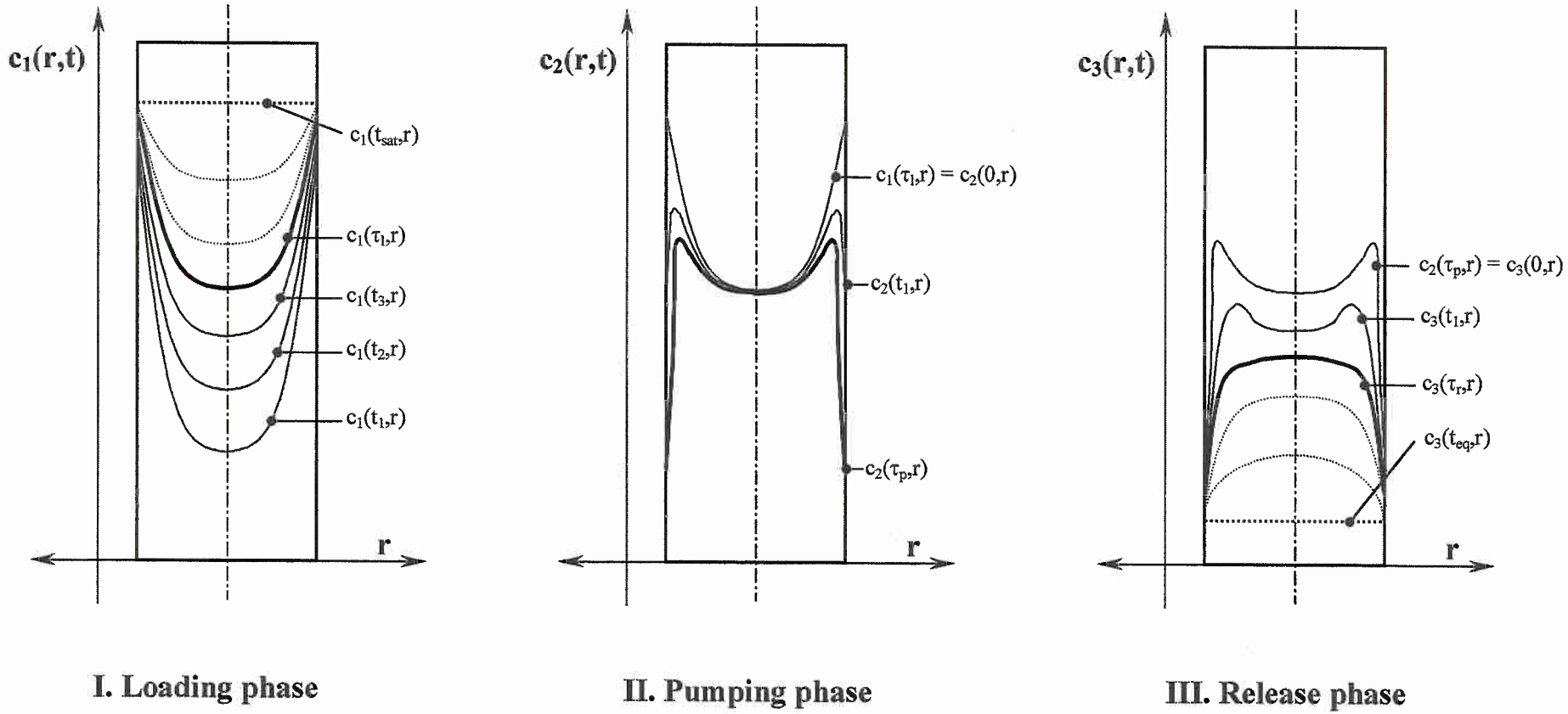

Figure 4. Hydrogen concentration profiles in a non-stationary sequence of the three experimental phases. The concentration profiles depicted in solid lines show the evolution of concentration with time during each phase. The wide line indicates the profile configured at the end of each phase, the dashed line show the progression the concentration profiles would follow till equilibrium situation in case of long enough time was allowed.

4. THEORETICAL APPROACH

4.1. Diffusive gas transport properties

4.1.1. Solubility

The amount of gas dissolved into the volume unit of solid in equilibrium at a certain pressure and temperature is referred to as the solubility S (mol m^{-3}) of the gas in the solid. It is described by the Sieverts' law:

$$S = K_{s,eff} p^{1/2} \tag{1}$$

which states that the gas solubility in a material is proportional to the square root of the external gas partial pressure, p (Pa), through the temperature dependent effective Sieverts' constant, $K_{s,eff}$ (mol m^{-3} $Pa^{-1/2}$).

The effective Sieverts' constant takes into account the fact that H atoms can be solved both in lattice interstitial sites and trapping centres (e.g. inclusions, dislocations, grain boundaries). Trapping has greater importance in the lower temperature range (around 873 K and lower for tungsten); its effect on H solubility is a net increase in the gas absorbed inventory and, consequently, an increase in the effective Sieverts' constant, $K_{s,eff}$, in comparison with lattice Sieverts' constant, K_s, which accounts only for the H inventory dissolved in the matrix interstitial sites [16]:

$$K_{s,eff} = K_s\left(1 + \frac{N_t}{N_l}\exp\left(\frac{E_t}{RT}\right)\right) \tag{2}$$

where N_t (m^{-3}) is the trap sites concentration, N_l (m^{-3}) the lattice dissolution sites concentration and E_t ($J \cdot mol^{-1}$) the average trapping activation energy. The temperature dependence of lattice Sieverts' constant may be described by an Arrhenius equation:

$$K_s = K_{s0}\exp\left(\frac{-E_s}{RT}\right) \tag{3}$$

K_{s0} (mol $m^{-3}Pa^{-1/2}$) being the pre-exponential factor, R (J $K^{-1}mol^{-1}$) the ideal gas constant and E_s (J mol^{-1}) the activation energy of the solution process. Depending on the sign of the solution energy, E_s, the material is characterised as endothermic or exothermic, when E_s is positive or negative respectively.

4.1.2. Diffusion

The first Fick's law accounts for a diffusive flux of gas through a solid lattice due to a gradient concentration through the spatial co-ordinate. In the absence of source terms and temperature gradients it can be expressed as follows:

$$\vec{J}(\vec{r},t) = -D_{eff}\vec{\nabla}c(\vec{r},t) \tag{4}$$

where $\vec{J}(\vec{r},t)$ (mol m^{-2} s^{-1}) is the H diffusive local flux dependent on time t and the position within the material $\vec{r}$, $c(\vec{r},t)$ (mol m^{-3}) is the local H concentration in the material and D_{eff} (m^2s^{-1}) is the effective diffusivity. When taking into consideration the continuity equation in such conditions, expressing that every increase of the gas concentration in a differential volume is due to a net inlet of diffusive flux:

$$\frac{\partial c(\vec{r},t)}{\partial t} = -\vec{\nabla}\vec{J}(\vec{r},t) \tag{5}$$

the second Fick's law is derived:

$$\frac{\partial c(\vec{r},t)}{\partial t} = D_{eff}\nabla^2 c(\vec{r},t) \tag{6}$$

where the analysed material has been considered isotropic and homogeneous when evaluating the effective diffusivity. Furthermore this parameter has been supposed to be independent of the local concentration (dilution approximation). In the same manner as the effective Sieverts' constant, the effective diffusivity, D_{eff}, takes into account the trapping effect; this process provokes the slowing down of the dynamics of transport decreasing the effective diffusivity from the lattice diffusivity value, D, which defines the H migration through a lattice free of any imperfection [16]:

$$D_{eff} = \frac{D}{\left(1 + \frac{N_t}{N_l}\exp\left(\frac{E_t}{RT}\right)\right)} \tag{7}$$

The lattice diffusivity, D, behaves in an Arrhenius manner with respect to temperature variation:

$$D = D_0\exp\left(\frac{-E_d}{RT}\right) \tag{8}$$

D_0 (m^2s^{-1}) being the pre-exponential diffusivity and E_d (J mol^{-1}) the activation energy for diffusion.

4.2. Non-stationary desorption modelling.

In previous reports [13,14], when modelling IDE experiments an stationary theoretical model was used, because H transport kinematics in the measured material was fast enough to assure equilibrium between the pressure of molecular H in the experimental chamber, V1, and the dissolved H in the specimens, both at the end of the loading phase and release phase within reasonable periods of time.

In contrast, tungsten presents such slow H transport kinematics that the experience carried out till final equilibrium situation would take too long (weeks) to maintain the stability of measuring devices. That is the reason why IDE have been envisaged with shorter periods of loading and release times, without reaching final equilibrium states, and accordingly modelled. The theoretical model applied here is similar to that developed in an earlier work [15]. Here, we have assumed additional simplifications taking into account that surface reactions proceed instantaneously in comparison to diffusion, thereby any time dependence of the boundary conditions was eliminated.

The model solves the diffusion equation in an infinite cylinder geometry linking all the three phases (loading, pumping and release). Considering the existing symmetries of the problem, only the radial co-ordinate remains in the ∇^2 operator in second Fick's law (6):

$$\frac{\partial c(r,t)}{\partial t} = D_{eff}\frac{1}{r}\frac{\partial}{\partial r}\left(r\frac{\partial c(r,t)}{\partial r}\right) \qquad (9)$$

The general solution of the previous equation for a certain initial concentration distribution $c(r,0)=f(r)$ and a constant boundary concentration, $c(r_{surface},t)=cte.$, can be found in [17] (page 66).

For the present case, in the loading phase the concentration distribution, $c_l(r,t)$, is obtained from the general solution of (9) assuming the following initial and boundary conditions:

$$c_l(r,0)=0 \quad \text{for } 0<r<a$$
$$c_l(a,t)=c_L \quad \text{for } 0<t<\tau_l \qquad (10)$$

a being the cylinder radius and c_L the H concentration at the sub-surface of the cylinder evaluated by means of Sieverts' law (1), $c_L=K_{s,eff}\cdot p_l$. With these boundary conditions (10), equation (9) has the following solution:

$$c_1(r,t) = c_L\left(1 - \frac{2}{a}\sum_{n=1}^{\infty}\frac{1}{\alpha_n}\frac{J_0(r\alpha_n)}{J_1(a\alpha_n)}\exp\left(-D_{eff}\alpha_n^{\,2}t\right)\right) \tag{11}$$

where $J_k(x)$ are the Bessel functions of the first kind and order k, while α_n (n=1,2,...) are the infinite real roots of the equation $J_0(a\alpha_n) = 0$.

The normalised concentration profiles, $c_1(r,t)/c_L$, built up during the loading phase are showed in Figure 5.

For the pumping phase, assuming the following boundary and initial conditions:

$$c_2(a,t)=0 \quad \text{for } 0<t<\tau_p$$
$$c_2(r,0)=c_1(r,\tau_l) \quad \text{for } 0<r<a \tag{12}$$

$c_2(r,t)$ is obtained as:

$$c_2(r,t) = \frac{2c_L}{a}\sum_{n=1}^{\infty}\frac{1}{\alpha_n}\frac{J_0(r\alpha_n)}{J_1(a\alpha_n)}\left[1-\exp\left(-D_{eff}\alpha_n^{\,2}\tau_1\right)\right]\exp\left(-D\alpha_n^{\,2}t\right) \tag{13}$$

The concentration profiles developed during the pumping phase are showed in Figure 6.

For the release phase, the following boundary and initial conditions are supposed to be fulfilled:

$$c_3(a,t)=c_f \quad \text{for } 0<t<\tau_r$$
$$c_3(r,0)=c_2(r,\tau_p) \quad \text{for } 0<r<a \tag{14}$$

c_f being the H concentration at the sub-surface of the cylinder evaluated as $c_f=K_{s,eff}p_f$. Solving again (9) with the previous conditions (14), $c_3(r,t)$ is obtained as:

$$c_3(r,t) = c_f + \frac{2}{a}\sum_{n=1}^{\infty}\frac{1}{\alpha_n}\frac{J_0(r\alpha_n)}{J_1(a\alpha_n)}\exp\left(-D_{eff}\alpha_n^{\,2}t\right)\left[c_L\left(1-\exp\left(-D_{eff}\alpha_n^{\,2}\tau_1\right)\right)\exp\left(-D_{eff}\alpha_n^{\,2}(\tau_p)\right)-c_f\right] \tag{15}$$

The evolution of the normalised concentration profiles, $c_3(r,t)/c_L$ during the loading phase is showed in Figure 7.

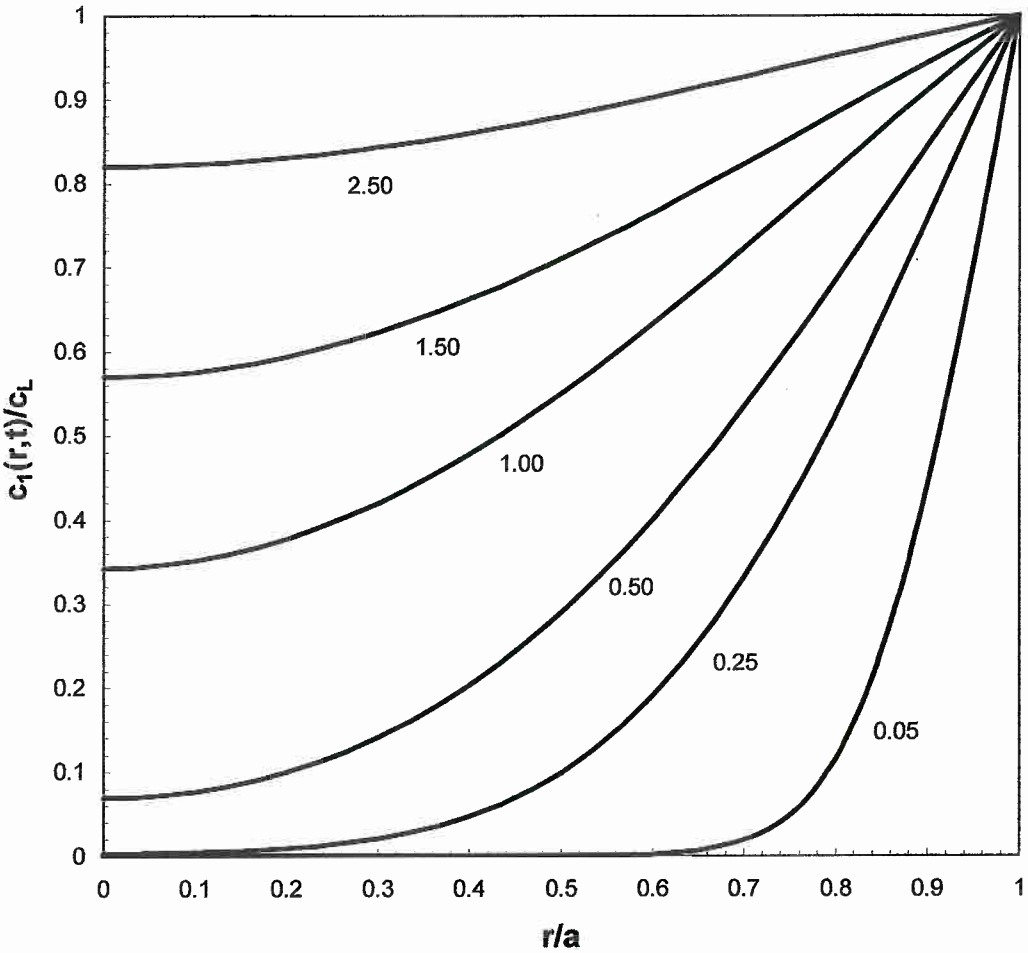

Figure 5. Hydrogen concentration profiles during the loading phase. Each curve corresponds to a period of time indicated by the number enclosed equalling t/τ_l. The curves refer to the following values: $D=5.117\cdot10^{-11}$ m^2s^{-1} (corresponding to H_P in tungsten at 673 K), τ_l=20000 s.

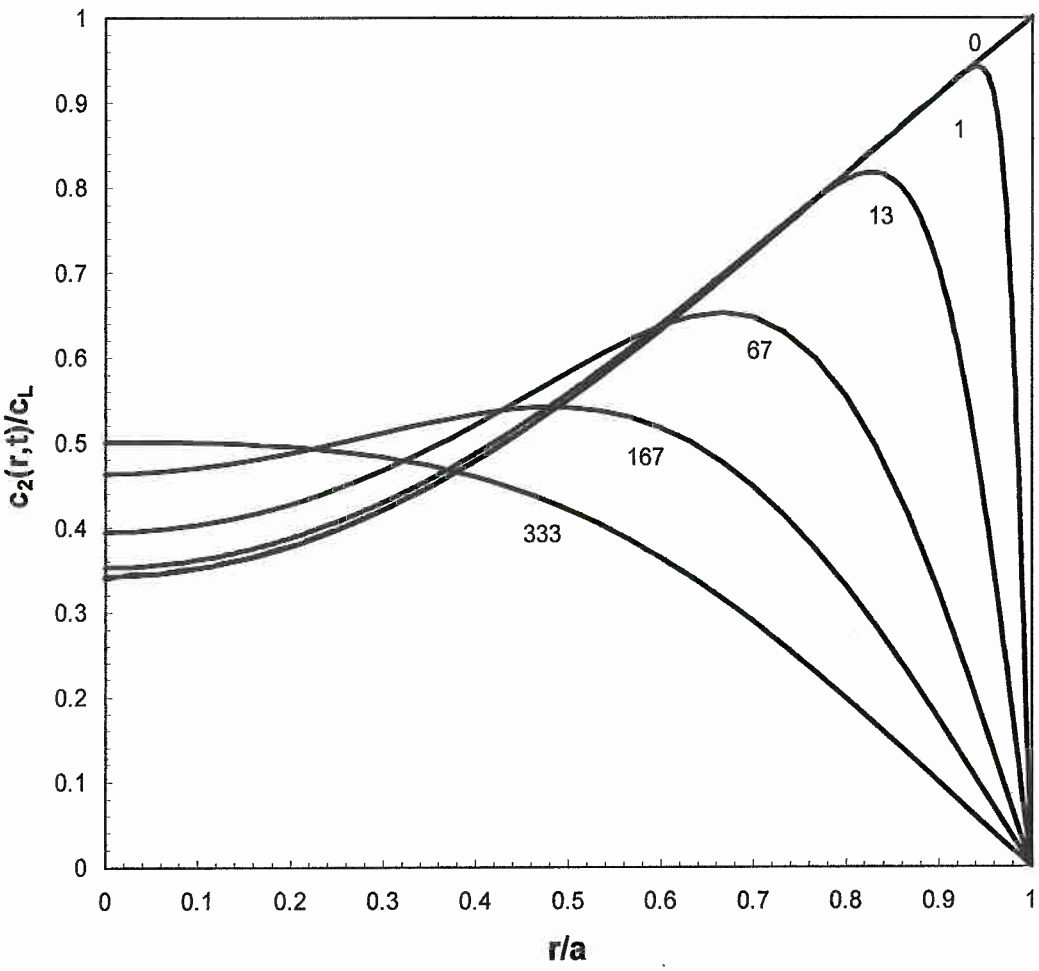

Figure 6. Hydrogen concentration profiles during the pumping phase. Each curve corresponds to a period of time indicated by the number enclosed equalling t/τ_p. The curves refer to the following values: $D=5.117\cdot10^{-11}$ m^2s^{-1}, $\tau_l=20000$ s, $\tau_p=30$ s.

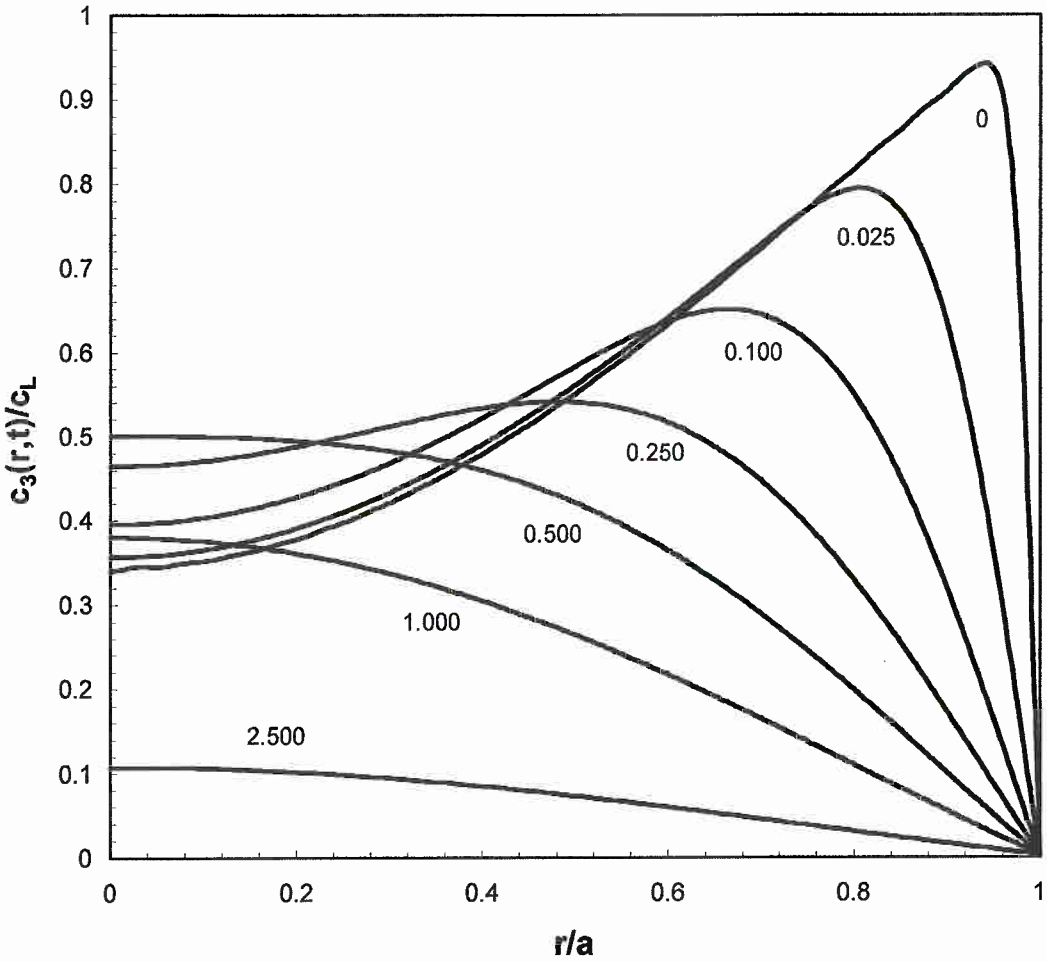

Figure 7. Hydrogen concentration profiles during the release phase. Each curve corresponds to a period of time indicated by the number enclosed equalling t/τ_r. The curves refer to the following values: $D=5.117\cdot10^{-11}$ m^2s^{-1}, τ_l=20000 s, τ_p=30 s, τ_r=20000 s, $p_f/p_l = 4.5\cdot10^{-6}$.

Once the $c_3(r,t)$ concentration distribution is determined, the H radial flux through the specimen surface can be derived from eq. (4) as:

$$J(t) = -D_{eff} \left. \frac{\partial c_3(r,t)}{\partial r} \right|_{r=a} \tag{16}$$

leading to the following expression:

$$J(t) = \frac{2D_{eff}}{a} \sum_{n=1}^{\infty} \exp\left(-D_{eff}\alpha_n^2 t\right)\left[c_L\left(1-\exp\left(-D_{eff}\alpha_n^2\tau_l\right)\right)\exp\left(-D_{eff}\alpha_n^2\left(\tau_p\right)\right)-c_f\right] \tag{17}$$

The amount of H released in a given time through the lateral area of the cylinder is evaluated as:

$$M(t) = 2\pi a h \int_0^t J(t')dt' \tag{18}$$

h being the height of the specimen.

Taking into account the calibrated volume of the chamber, V, the theoretical expression for the measured pressure is:

$$p(t) = \frac{RT}{(V-4V_s)} 4\pi h \sum_{n=1}^{\infty} \frac{1}{\alpha_n^2}\left(1-\exp\left(-D_{eff}\alpha_n^2 t\right)\right)\left(c_L\left(1-\exp\left(-D_{eff}\alpha_n^2\tau_l\right)\right)\exp\left(-D_{eff}\alpha_n^2\tau_p\right)-c_f\right) \tag{19}$$

where V_s is the volume of one specimen.

Considering Sieverts' law for c_L and c_f, expression (19) can be expressed as function of direct experimental parameters (pressures and times) and the only unknown transport parameters D_{eff} and $K_{s,eff}$. Expression (19) is used in a non-linear least-squares fitting routine in order to derive the values of the effective transport parameters (D_{eff} and $K_{s,eff}$) at each experimental temperature, an example of a fitting is shown in (Figure 8).

4.3. Isotope effects

The quantum-statistical theory developed by Ebisuzaki et.al. [18] is the currently used to predict isotope effects in H-metal interactions. This theory applies vibration partition functions to the solution and diffusion processes assuming the following simplifying hypotheses:

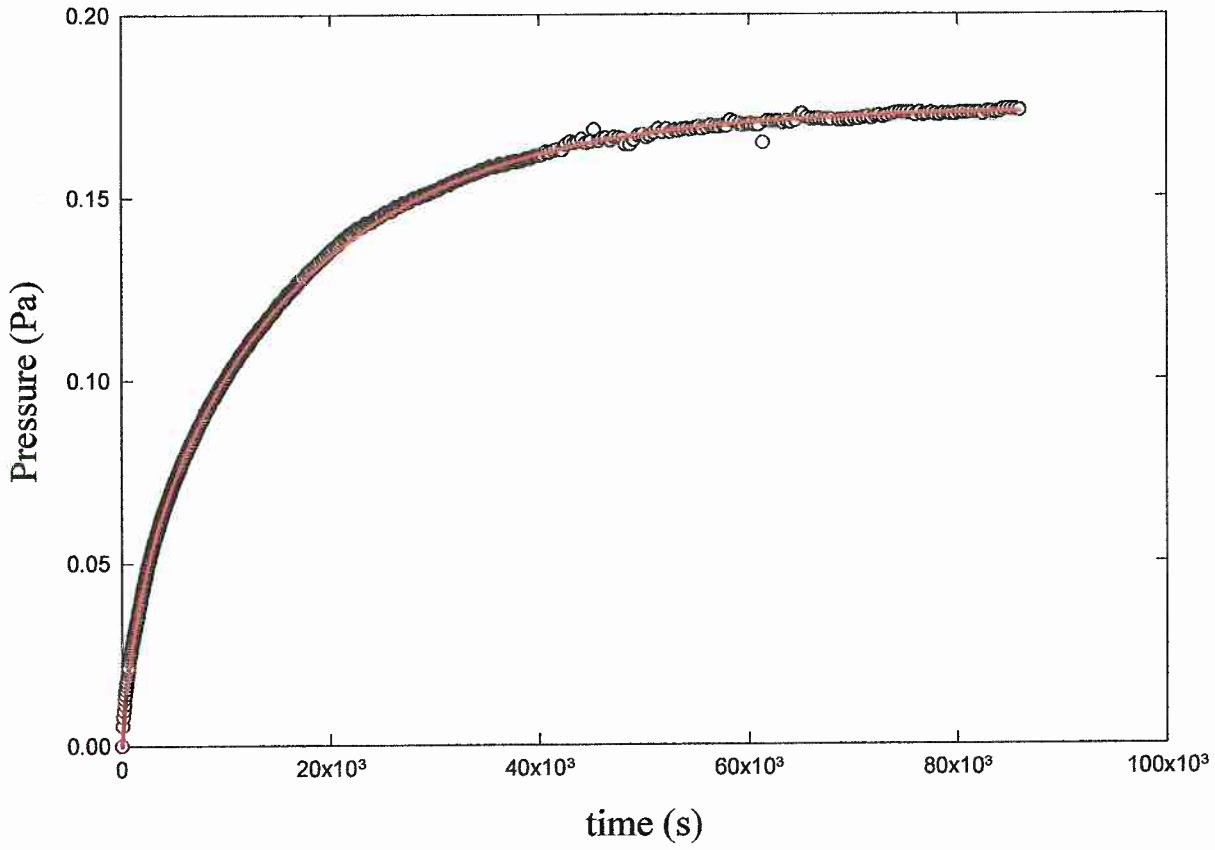

Figure 8. Experimental pressure increase ○ and fitting —.

- approximation to dilute solution; a wide range of experiments has confirmed that only a minor fraction of available solution sites N_I is occupied in the current experimental conditions.
- the metal is isotropic and homogeneous; the analysed material does not make any difference between specified directions from the transport point of view, whereas the homogeneity assumption allows obtaining the isotope effect on an averaged potential barrier-well configuration.
- the absorbed atoms behave in the potential wells as harmonic oscillators decoupled from the vibrations of the host-lattice atoms; this assumption allows limiting to three the number of localised modes of H vibration in the ground state and to two in the excited state.
- the vibrational frequencies are proportional to $m^{-1/2}$ where m is the mass of the absorbed atom; this is an implicit characteristic in a harmonic oscillator.

Under these hypotheses the isotope transformation of H transport parameters in a metal or alloy satisfies the following laws:

$$\ln\frac{K_{s\alpha}}{K_{s\beta}} = 3\left(\frac{f\left(\frac{\theta}{\sqrt{\beta}T}\right)}{f\left(\frac{\theta}{\sqrt{\alpha}T}\right)}\right) - \frac{3}{2}\ln\frac{\beta}{\alpha} + \frac{g^0{}_\alpha - g^0{}_\beta}{2RT} \tag{20}$$

$$\frac{D_\alpha}{D_\beta} = \sqrt{\frac{\beta}{\alpha}}\left(\frac{f\left(\frac{\theta}{\sqrt{\alpha}T}\right)}{f\left(\frac{\theta}{\sqrt{\beta}T}\right)}\right)^3\left(\frac{f\left(\frac{\theta^*}{\sqrt{\beta}T}\right)}{f\left(\frac{\theta^*}{\sqrt{\alpha}T}\right)}\right)^2 \tag{21}$$

α and β being the atomic mass 1, 2, 3 for each isotope protium (H_P), H_D and H_T, $g^0{}_\alpha$ and $g^0{}_\beta$ the molar free energies of the isotope gas diatomic molecules at reference state (298 K, 1 bar) [19], and f(x) the vibration partition function defined by:

$$f(x) = \frac{\sinh\left(\frac{x}{2}\right)}{\frac{x}{2}} \tag{22}$$

θ and θ^* are the characteristic vibration temperatures of H_P oscillation in the ground and excited state (i.e. in the bottom of the potential well and the top of the diffusion barrier), respectively; they are related to the vibration frequencies ν and ν^* (s^{-1}) by:

$$\theta = \frac{h\nu}{k}, \ \theta^* = \frac{h\nu^*}{k} \tag{23}$$

where h is the Planck constant (6.6260755 10^{-34} J s) and k is the Boltzmann constant (1.380658 10^{-23} J K^{-1}).

5. RESULTS AND DISCUSSION

5.1. Effective transport parameters

A series of measurements (loading-release) has been performed over the temperature range 673 to 1073 K; each one is composed of the run with the specimen and the corresponding blank run. The measurements have been carried out with H_P and H_D in order to account for any isotope effect on transport parameters. The loading pressure has been 10^5 Pa over the whole experimental temperature range, except for a final series performed with both isotopes at the temperature 873 K and different pressures (from 13.3 kPa to 101.3 kPa), to check for the validity of diffusion limited regime.

A non-liner least squares fitting routine is run for each measurement with eq. (19) as the function to reproduce the experimental pressure rise, and the effective transport parameters, D_{eff} and $K_{s,eff}$, as fitting variables.

The results are depicted in Figures 9 and 10. The values of permeability have been obtained from Richardson's law as $\Phi=D_{eff}\cdot K_{s,eff}$ (Figure 11).

The measurements carried out with H_D at the two lower temperatures have not lead to reliable fitted release curves, due to measuring stability. The higher temperature 1073 K has not been envisaged for H_D because in the previous measurement with H_P at that temperature an excessive dilatation of the platinum wire was observed, having been necessary to mend the Pt-resistance thermometer before further experimental exploration.

Trapping effects on experimental diffusivity and Sieverts' constant values are noticeable in figures 9 and 10; below approximately 873 K; Sieverts' constant values increase whereas diffusivity values diminish as it was theoretically stated in section 3.1.

A set of 4 measurements at the same temperature, 873 K, at different pressures 13, 33, 53, 101 kPa, have been performed to check for a possible influence of surface effects on the measurements. No significant variation in the obtained diffusivities was observed as the charging pressure varied (Figure 12). This fact indicates the predominance of a diffusive transport regime.

From this set of four measurements Sievert's law is verified; the proportional relation between solubility S and the square root of the H loading pressure is checked (Figure 13). This is an experimental verification of the H atomic dissolution into the

steel. It is worth noting that, by means of the non-stationary model developed here and with the loading-deloading times used (24 hours each), the tungsten specimens do not reach the saturation condition. Nevertheless, the model assumes that the final equilibrium concentration, c_L, is built up instantaneously at the sub-surface in the loading phase (what is true because any surface effect is absent); therefore, the solubility $S=c_L$, can be obtained directly in each run (eq. (19)).

5.2. Lattice transport parameters.

The obtained experimental data (Figures 9-11) can be fitted to the effective constant functions described by equations (2), (3), (7) and (8) obtaining all the transport parameters (E_s, K_{s0}, E_d, D_0, E_t, N_t). The calculation of these parameters is divided into two phases:

(1) obtaining the lattice constants D, K_s, and Φ;

(2) obtaining the trapping parameters E_t, N_t.

The model of the experimental pressure increase has as fitting parameters the effective diffusivity and Sieverts' constant. Consequently, the lattice constants D and K_s are directly obtained from fitting the experimental values ($D_{eff,\,i}$ and $K_{s,eff,\,i}$) to an Arrhenius trend in the proper temperature range, i.e. above 873 K where trapping effects are negligible.

E_d and D_0 are the fitting parameters for the lattice diffusivity (Figure 14); the displayed r-squared value, R^2, accounting for the fitting quality.

The resultant lattice diffusivity for H_P is:

$$D(m^2s^{-1})=5.682\cdot10^{-10}\exp(-9278/RT)$$

For H_D:

$$D(m^2s^{-1})=5.490\cdot10^{-10}\exp(-9995/RT).$$

For the lattice Sieverts' constant E_s and K_{s0} are the fitting parameters (Figure 15).

The resultant Sieverts' constant for H_P is:

$$K_s(mol\ m^{-3}Pa^{-1/2})=2.896\cdot10^{-2}\ \exp(-26879/RT)$$

For H_D:

$$K_s(mol\ m^{-3}Pa^{-1/2})=2.748\cdot10^{-2}\ \exp(-28740/RT)$$

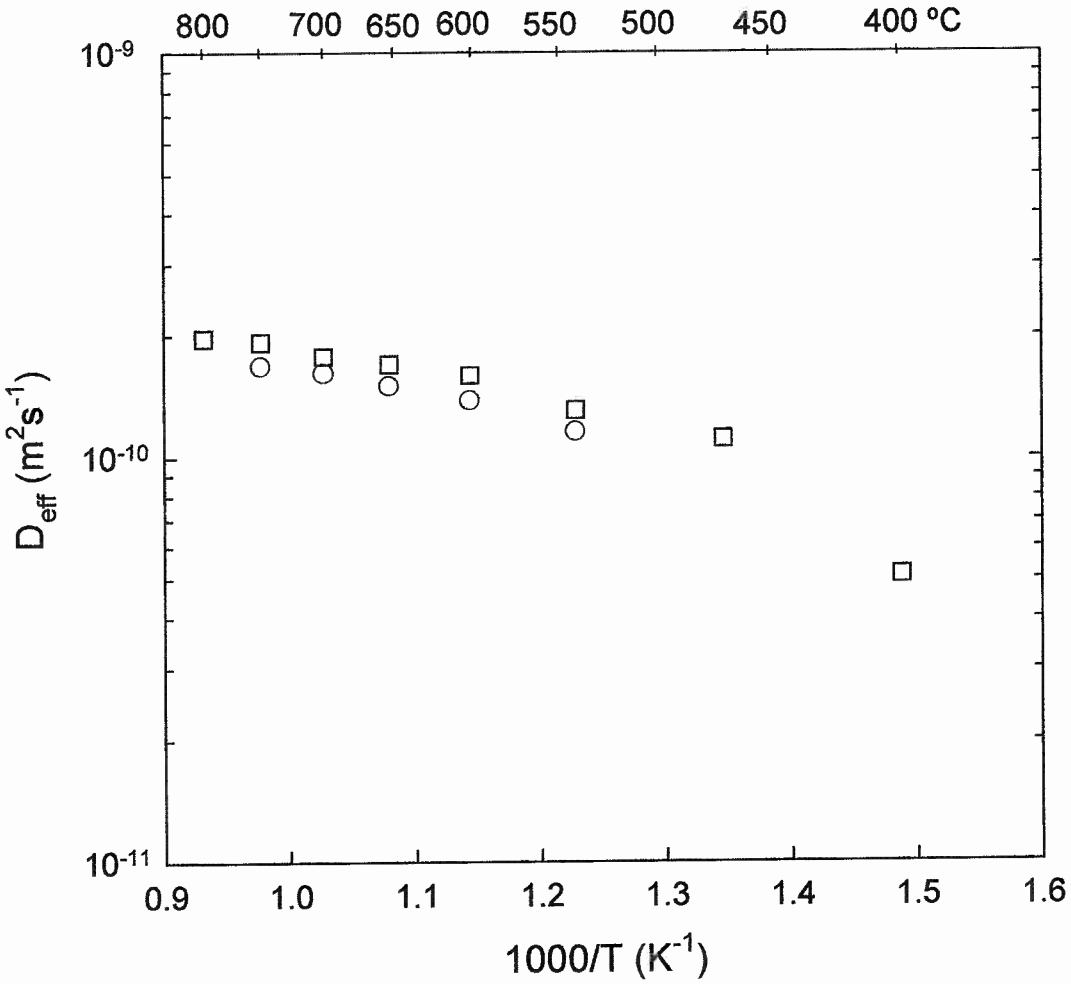

Figure 9. Arrhenius plot of effective diffusivities: the squared points correspond to protium, the circled ones to deuterium.

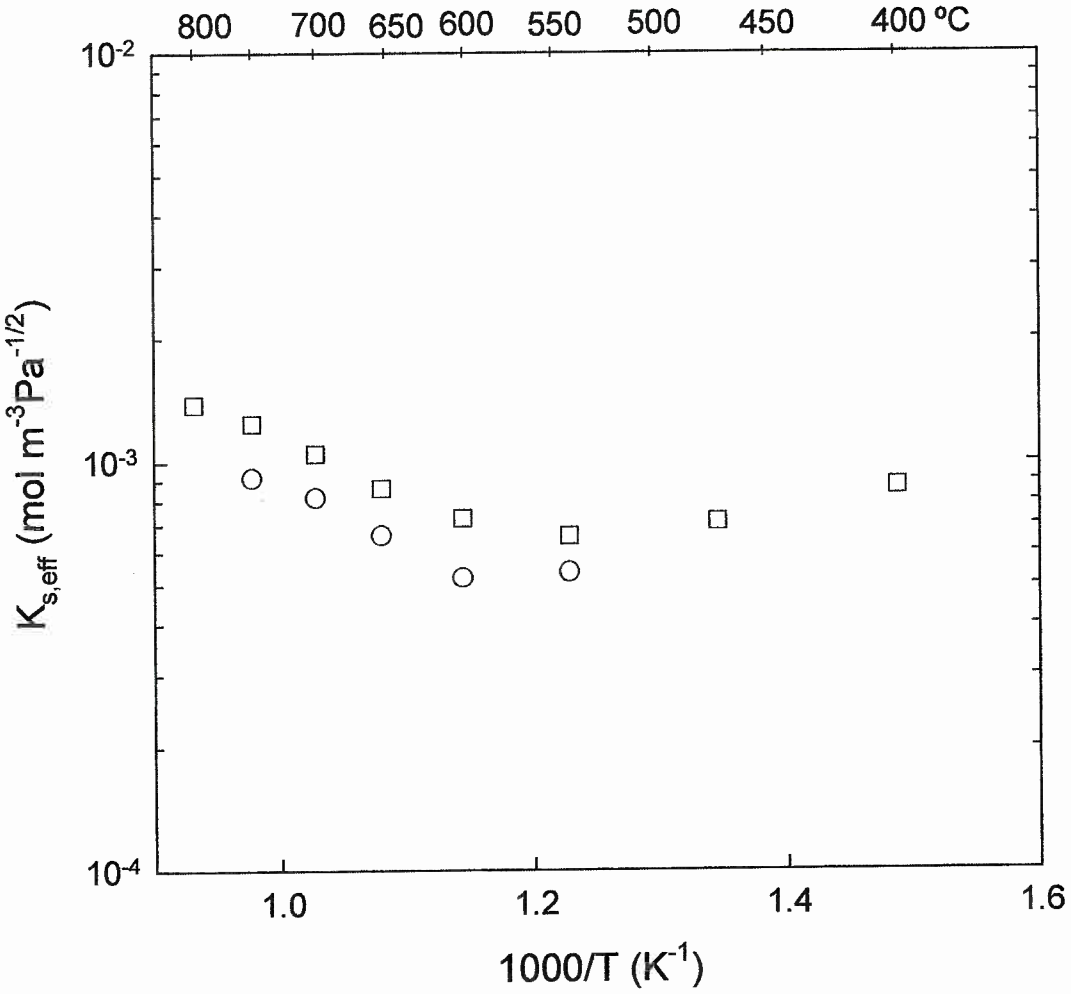

Figure 10. Arrhenius plot of effective Sieverts' constants: the squared points correspond to protium, the circled ones to deuterium.

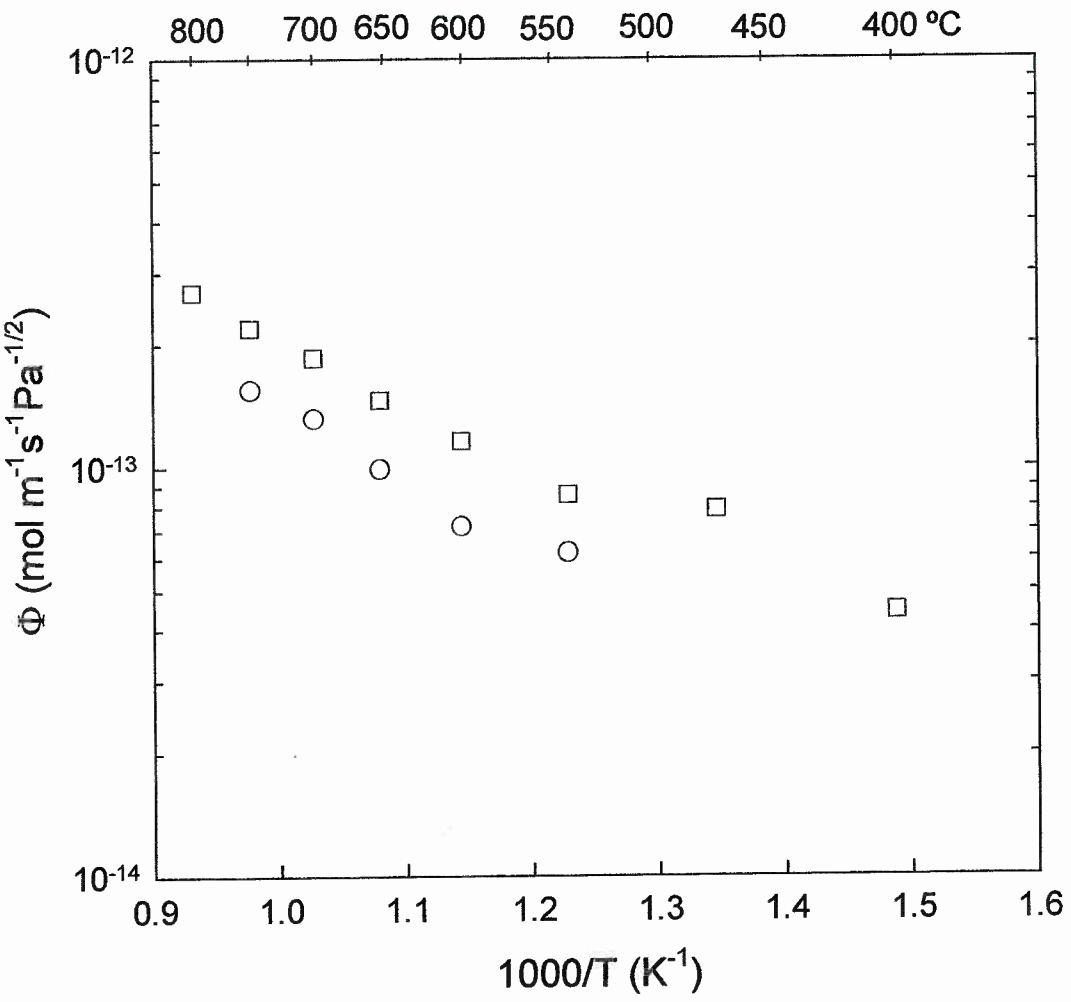

Figure 11. Arrhenius plot of effective permeabilities: the squared points correspond to protium, the circled ones to deuterium.

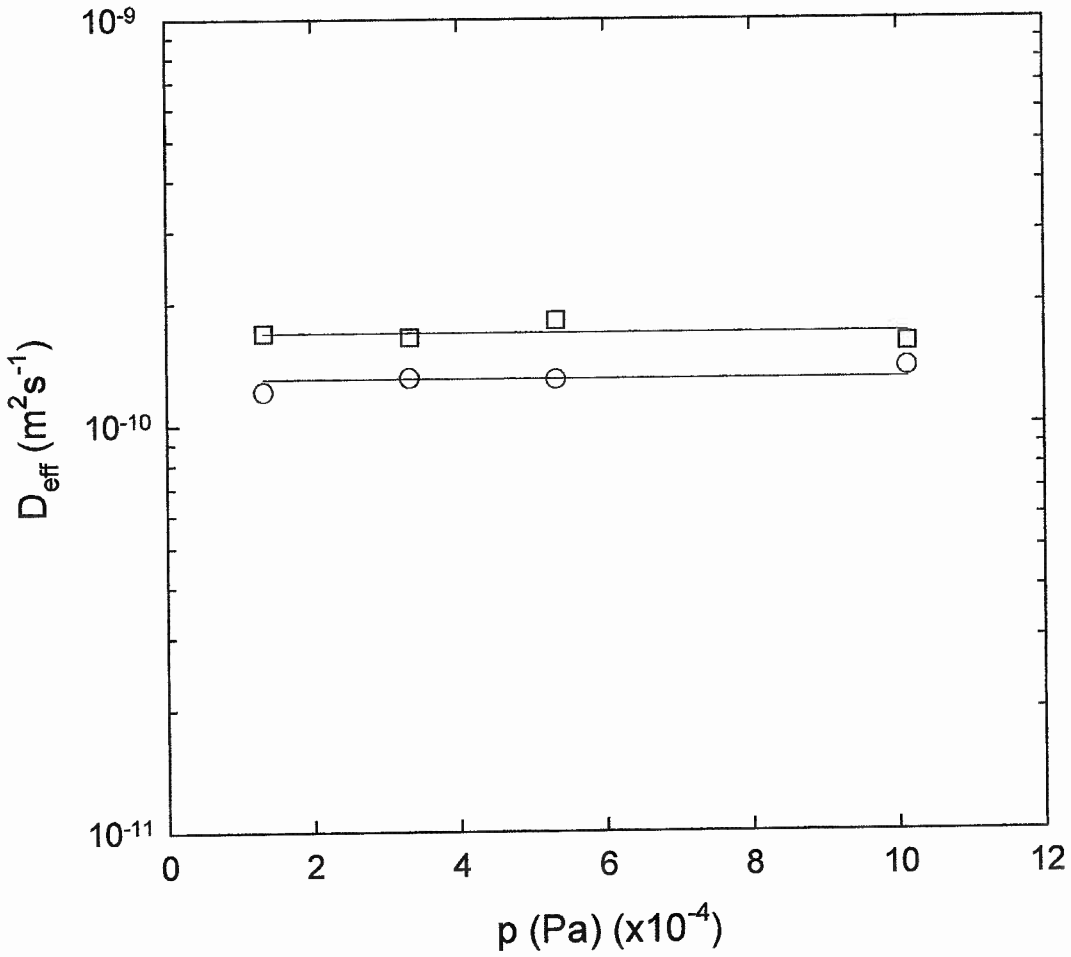

Figure 12. Diffusivities for 873 K at different loading pressures. Surface effect negligible. The squared points correspond to protium, the circled ones to deuterium.

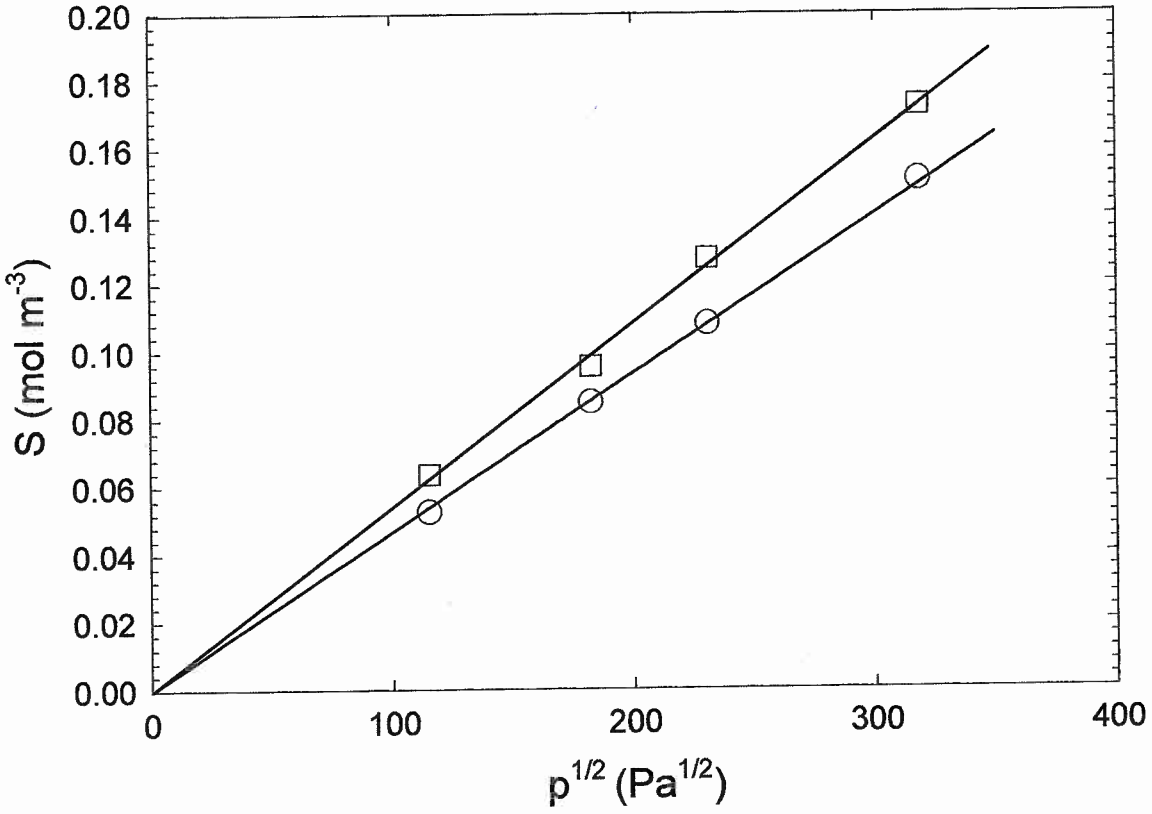

Figure 13. Solubilities for 873 K at different loading pressures. Sieverts' law verification. The squared points correspond to protium, the circled ones to deuterium.

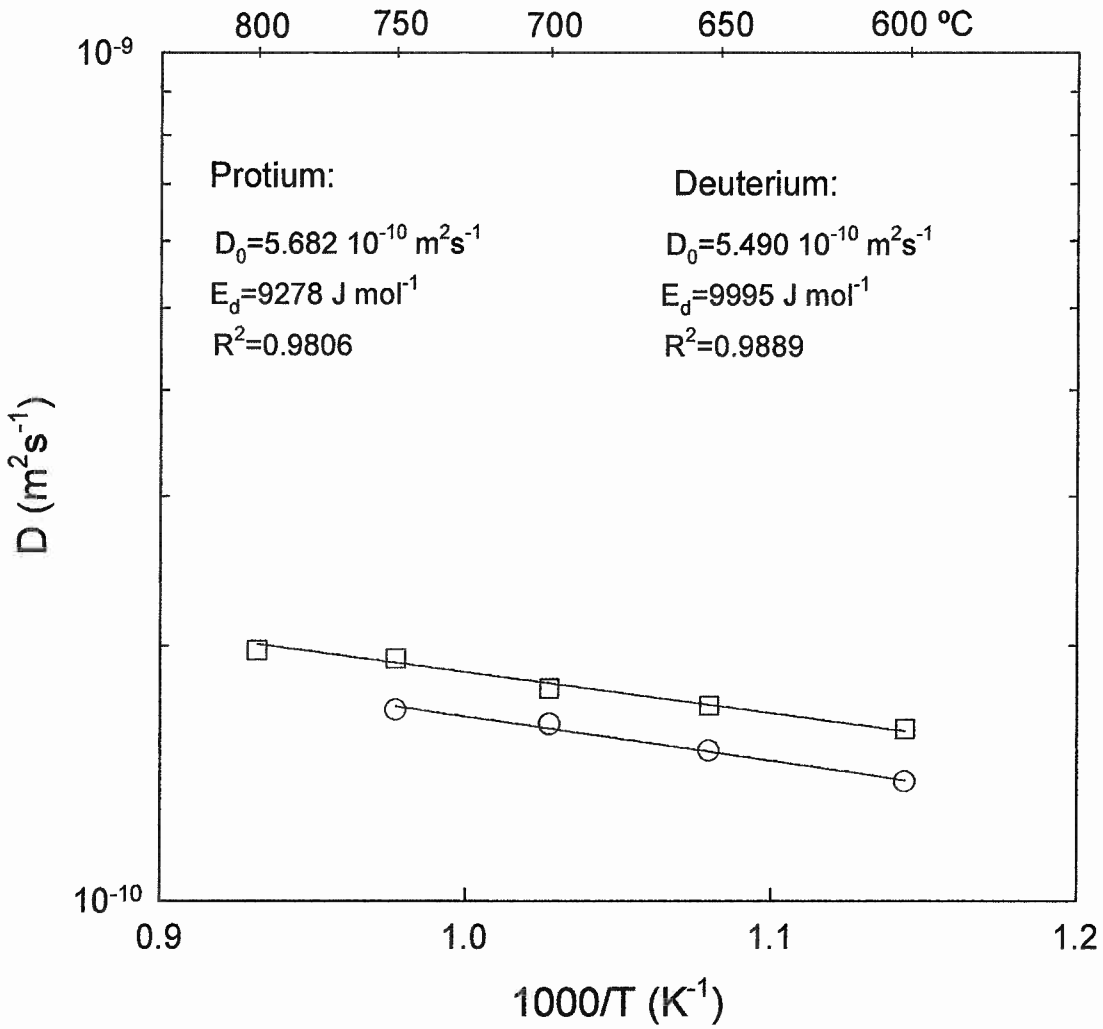

Figure 14. Arrhenius plot of the fitted lattice diffusivities.

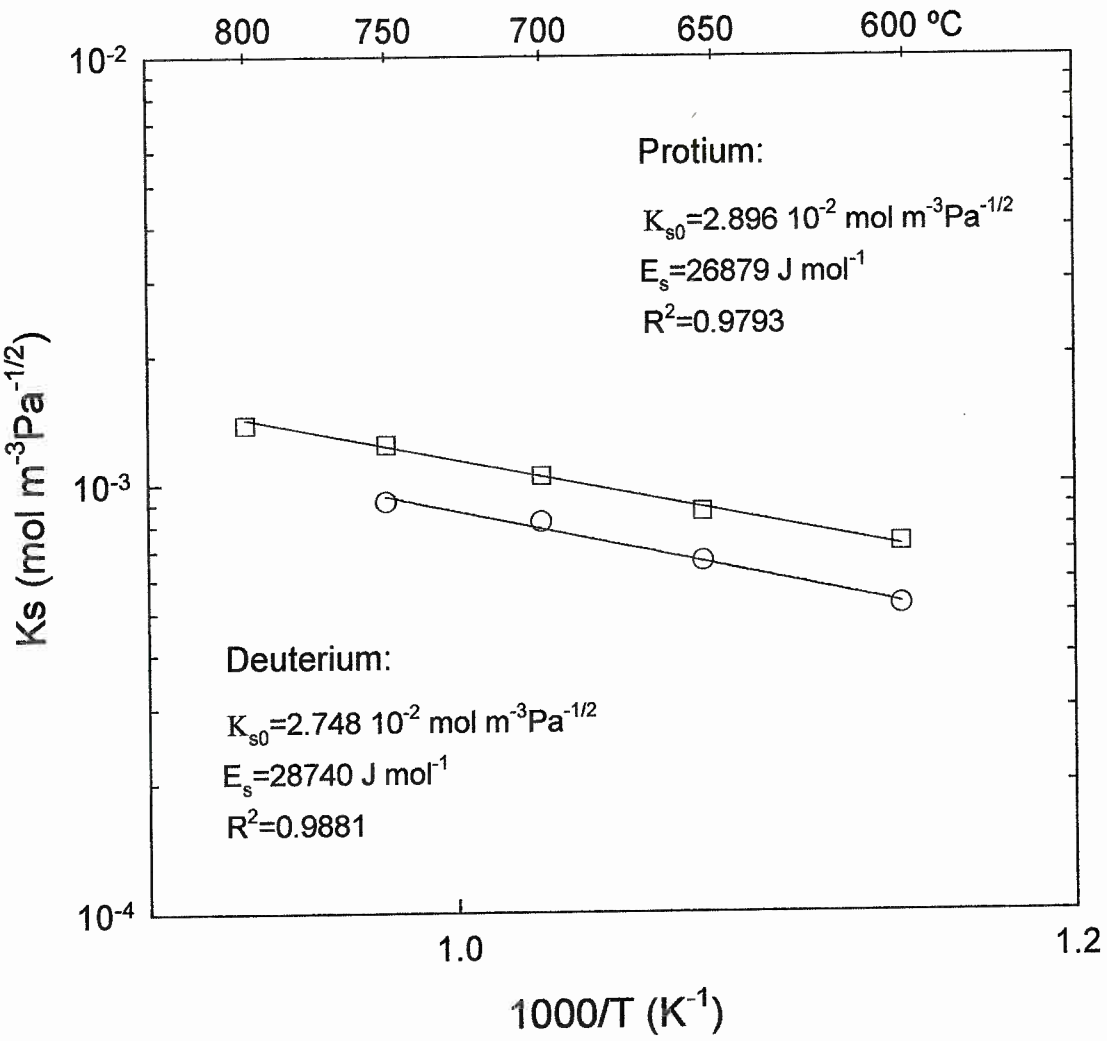

Figure 15. Arrhenius plot of the fitted lattice Sieverts' constants.

The permeability, Φ, is subsequently obtained as the product of the previous lattice diffusivities and Sieverts' constant: $\Phi=D\cdot K_s$ (Richardson's law); i.e. the permeation energy is obtained as $E_p=E_s+E_d$, whereas the pre-exponential permeability constant is evaluated as $\Phi_0=D_0\cdot Ks_0$. The result is plotted in Figure 16.

The derived permeability for H_P is:

$$\Phi(\text{mol m}^{-1}\text{Pa}^{-1/2}\text{s}^{-1})=1.645\cdot10^{-11}\exp(-36158/RT)$$

For H_D:

$$\Phi(\text{mol m}^{-1}\text{Pa}^{-1/2}\text{s}^{-1})=1.508\cdot10^{-11}\exp(-38736/RT).$$

It is worth remarking that permeability values do not come from a fitting with experimentally values, but from the product of K_s and D constants. In Figure 16 it can be noticed how the derived Arrhenius tendency for permeability corresponds well to the individual points derived as $\Phi_i=(K_{s,eff,\ i}\cdot D_{eff,\ i})$, at high temperatures. As the temperature decreases the Arrhenius law match worse the individual points. The reason for this may be the fact that, at lower temperatures, the gas outgassing from the chamber walls acquires more importance in comparison with the gas deloaded from the specimens, as a result the assumed error in the measurement increases and the dispersion of the experimental points around the general law is larger.

5.3. Trapping parameters

The characteristic trapping parameters of the specimen can be obtained from the previous lattice parameters and the experimental data obtained over the trapping temperature range. A non-linear fitting routine has been run for effective parameters with equations (2) and (7) as fitting functions, N_t/N_s and E_t being the fitting parameters. The results are plotted in Fig. 17 and 18. The χ^2 parameter shows the quality of the non-linear fitting routine.

The obtained trapping parameters for H_P are:

$$N_t/N_s=5.29\cdot10^{-7},\ E_t=86586\ \text{J mol}^{-1}$$

For H_D:

$$N_t/N_s=2.55\cdot10^{-7},\ E_t=93658\ \text{J mol}^{-1}$$

It should be noted that the trapping H_D parameters must be taken with caution because only one experimental run has been successfully modelled within the trapping range.

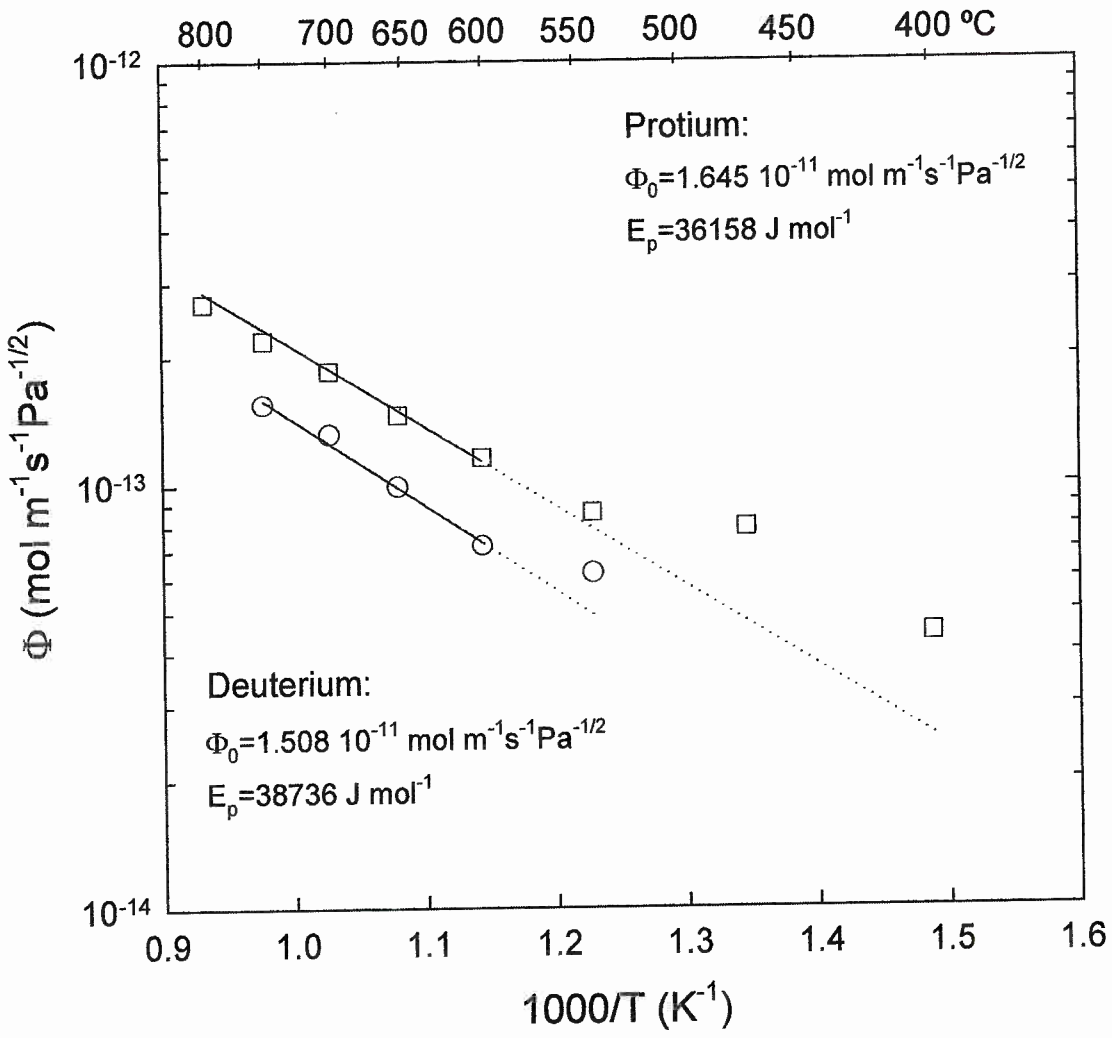

Figure 16. Arrhenius plot of the permeabilities.

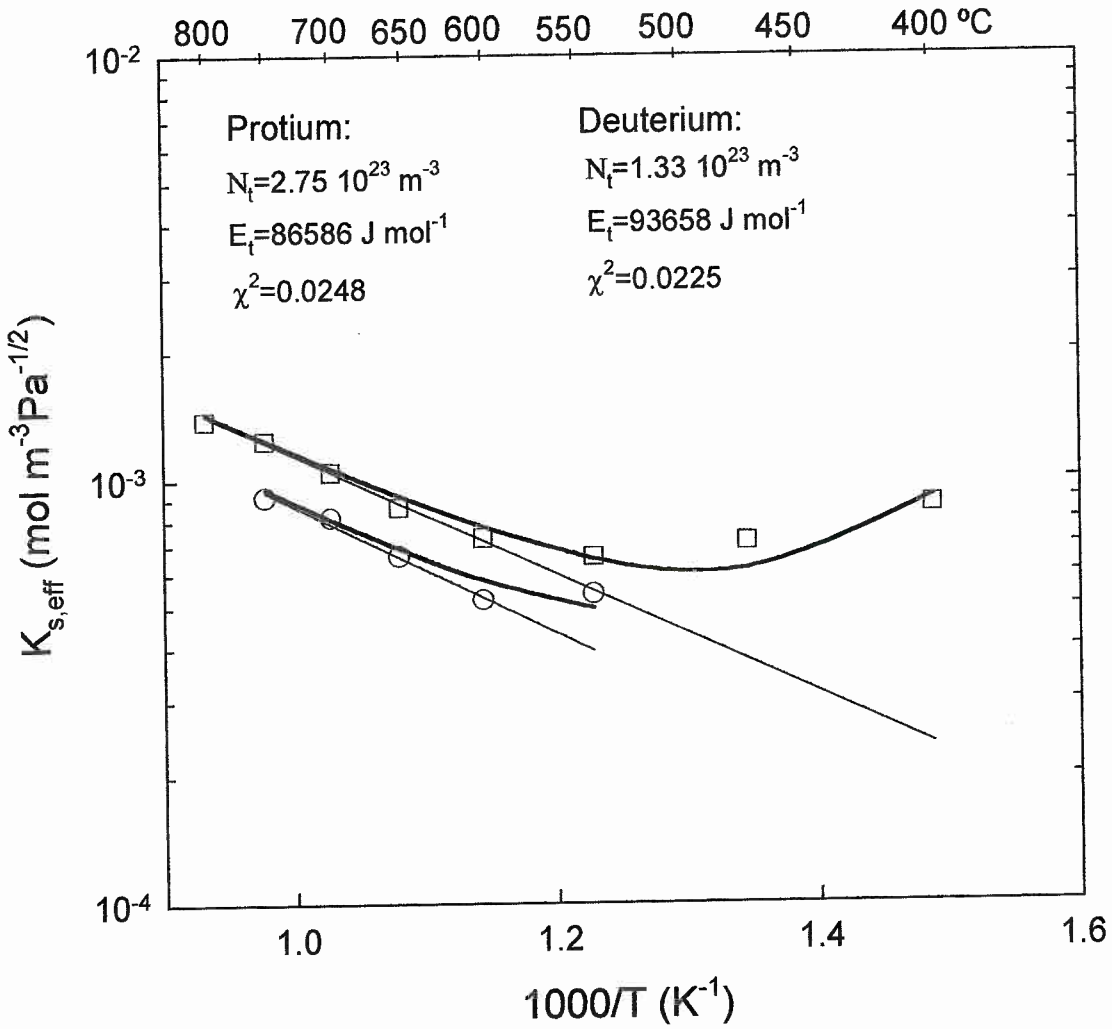

Figure 17. Fitted effective Sieverts' constants, trapping parameters evaluation. The squared points correspond to protium, the circled ones to deuterium. The straight lines represent the respective lattice parameters.

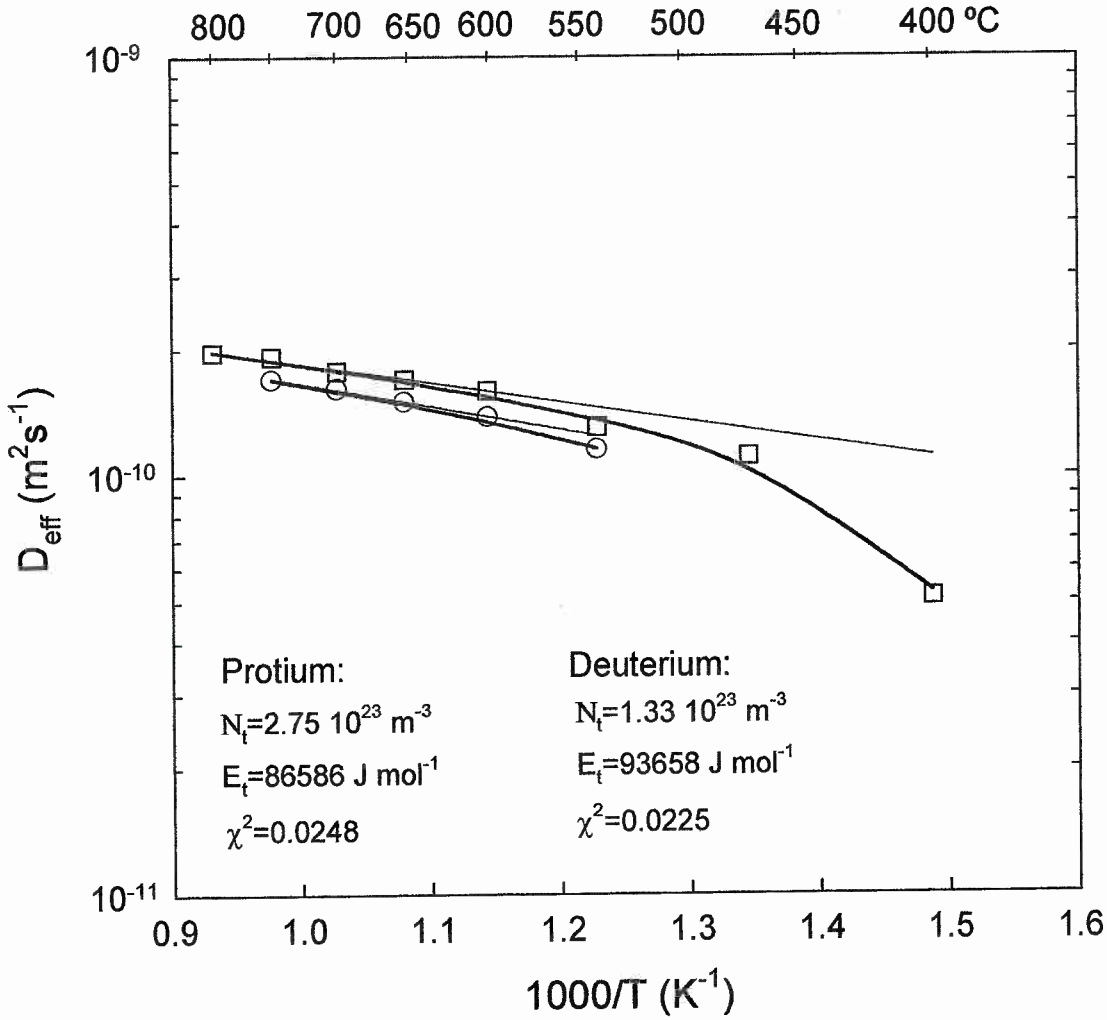

Figure 18. Fitted effective diffusivities, trapping parameters evaluation. The squared points correspond to protium, the circled ones to deuterium. The straight lines represent the respective lattice parameters.

The value of 5.2 10^{29} sites m^{-3} has been taken for the density of solution sites into the lattice, N_l, because tungsten shows a body cubic centered structure, where H accommodates preferentially in the tetrahedral interstitial positions similarly to iron [20]; consequently, the density of trapping sites is N_t=2.75 10^{23} m^{-3} for H_P, N_t=1.33 10^{23} for H_D.

The experimentally obtained trapping energy, (86.6 kJ mol^{-1} for H_P, 93.7 kJ mol^{-1} for H_D), appears to be too high for dislocation or grain boundary traps. However, extensive trapping phenomenon with high trapping energies has been reported before for polycrystalline tungsten [10]. In that occasion it was suggested that H-H bonding, in H clusters nucleated at the structural defects of tungsten, could be the reason for such a high trapping energy. That hypothesis could also explain the results obtained for trapping in the present experiment.

5.4. Isotope effect and extrapolation to tritium

The isotope effect on transport parameters is studied in the experimental temperature range 873 K to 1073 K. A mean reduction in the effective diffusivity with a factor $D_{eff}(H_P)/D_{eff}(H_D)$=1.13, has been noticed when changing isotope from H_P to H_D, instead of the classical value 1.41. For Sieverts' constant a greater mean reduction is evaluated, $K_{s,eff}(H_P)/K_{s,eff}(H_D)$=1.29.

The quantum-statistical theory developed by Ebisuzaki et.al. [18] on isotope effects in H-metal interactions is used here. From the effective Sieverts' constant and diffusivity data obtained for H_D and H_P, the characteristic vibration temperatures of H_P are derived, by fitting equations (20) and (21), as:

$$\theta=893\ K,\ \theta^*=2467\ K$$

This vibration temperatures have been used to extrapolate the tritum Sieverts' constant and diffusivity (Figures 19 and 20). The complete set of diffusive transport parameters for H_T has been obtained as:

$$D(m^2s^{-1})=5.342\cdot10^{-10}\exp(-11166/RT),$$

$$K_s(mol\ m^{-3}Pa^{-1/2})=2.246\cdot10^{-2}\exp(-27751/RT),$$

$$\Phi(mol\ m^{-1}Pa^{-1/2}s^{-1})=1.200\cdot10^{-11}\exp(-38917/RT).$$

$$E_t(J/mol)=100453,\ N_t(sites/m^3)=3.22\ 10^{23}.$$

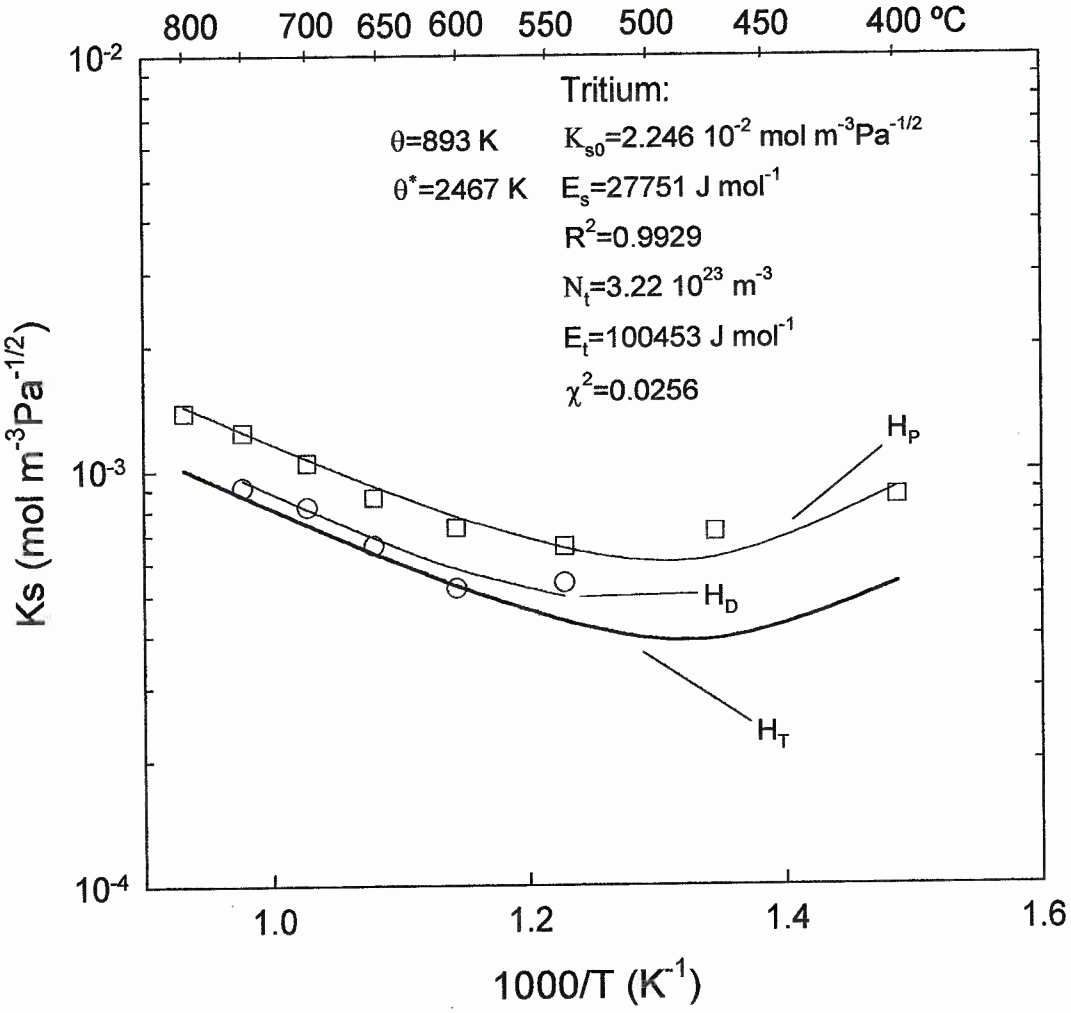

Figure 19. Arrhenius plot of hydrogen isotopes effective Sieverts' constant. Extrapolation to tritium.

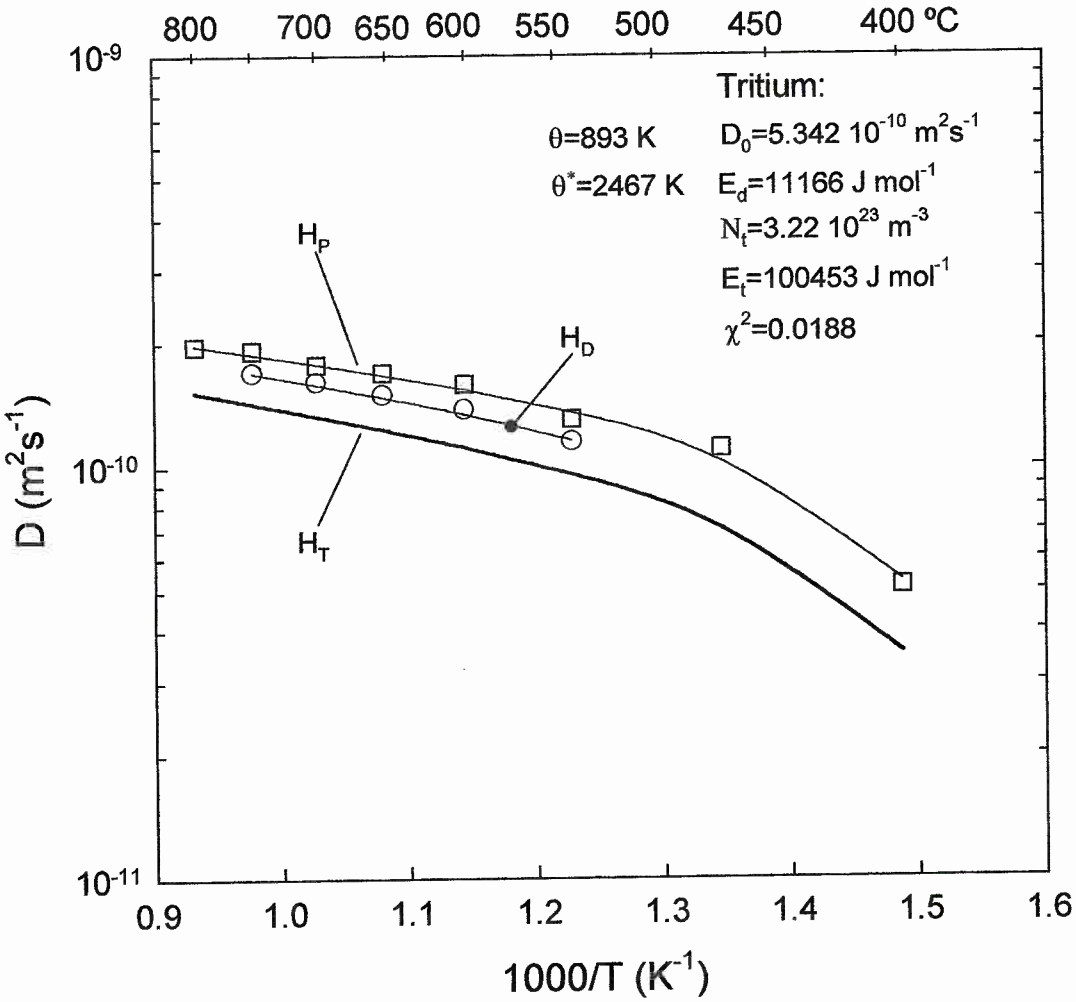

Figure 20. Arrhenius plot of hydrogen isotopes effective diffusivities. Extrapolation to tritium.

5.5. Comparison of results

In Figures 21-23 the obtained diffusive transport parameters are compared with the results reported elsewhere. A broad dispersion exists amongst all the results; the reason for such divergence can be found in the following features:

- In the experiments using W specimens at high temperatures [3,5,7] the H atomisation phenomenon may imply an underestimation of the evaluated molecular H inventories.

- The permeation technique [4,6,10] is more susceptible to surface reactions limiting the H transport than the gas desorption studies because in the first technique a great specimen surface for adsorption and recombination is present in comparison with very short diffusive paths. A very thin oxide layer may reduce the transport kinematics and host a non-negligible amount of H, leading to a Sieverts' constant overestimation and a diffusivity underestimation.

- The experiments using H ion implantation [8,9] to load the W specimens, provoke ion-induced traps so that the effective transport parameters may depart from those obtained in the presence of natural traps exclusively.

- The microstructure of each specimen experimented may influence the H transport within the bulk of tungsten. Moreover, depending on the manufacturing technique and subsequent heat treatment, the specimens show a particular microstructure with different grain sizes and different dislocation densities; these are sources of internal stress in the material where H may be trapped and even nucleate to form clusters.

- Other sources of variation may be the no-consideration of temperature transitory periods and long pumping down stages before the release phase study.

In terms of activation energies, the energy of diffusion, E_d, reported here (9.3 $kJ \cdot mol^{-1}$ H_P, 10.0 $kJ \cdot mol^{-1}$ H_D, 11.2 $kJ \cdot mol^{-1}$ H_T) is the lowest comparing to other referenced values. The solution energy here (26.9 $kJ \cdot mol^{-1}$ H_P, 28.7 $kJ \cdot mol^{-1}$ H_D, 27.8 $kJ \cdot mol^{-1}$ H_T), is close to that reported in [4]. With regard to trapping effect, the trap density values and the high trapping energies obtained approximate well the results obtained in [10].

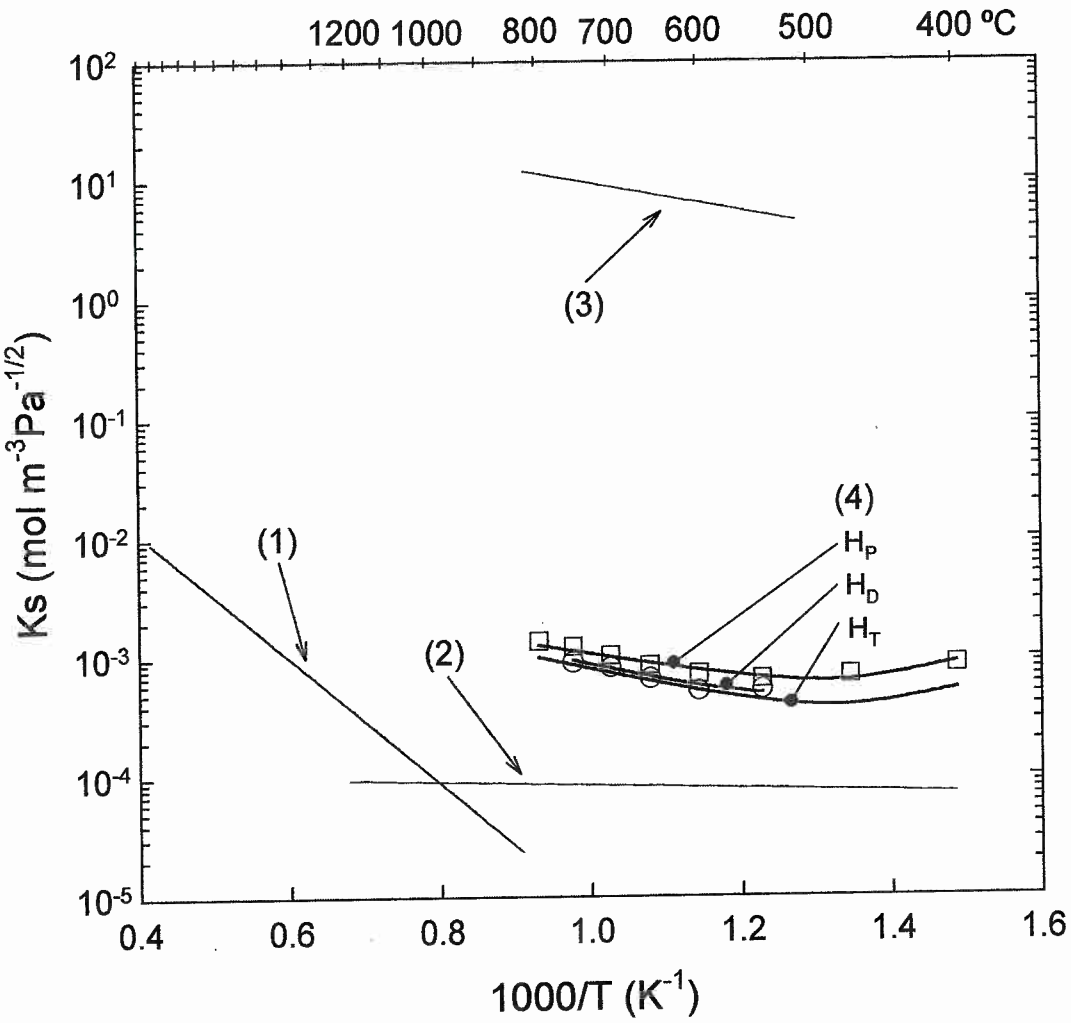

Figure 21. Hydrogen Sieverts' constant in tungsten: (1) Frauenfelder [3], (2) Zakharov et.al. [6], (3) Kizu et.al. [4], (4) This work.

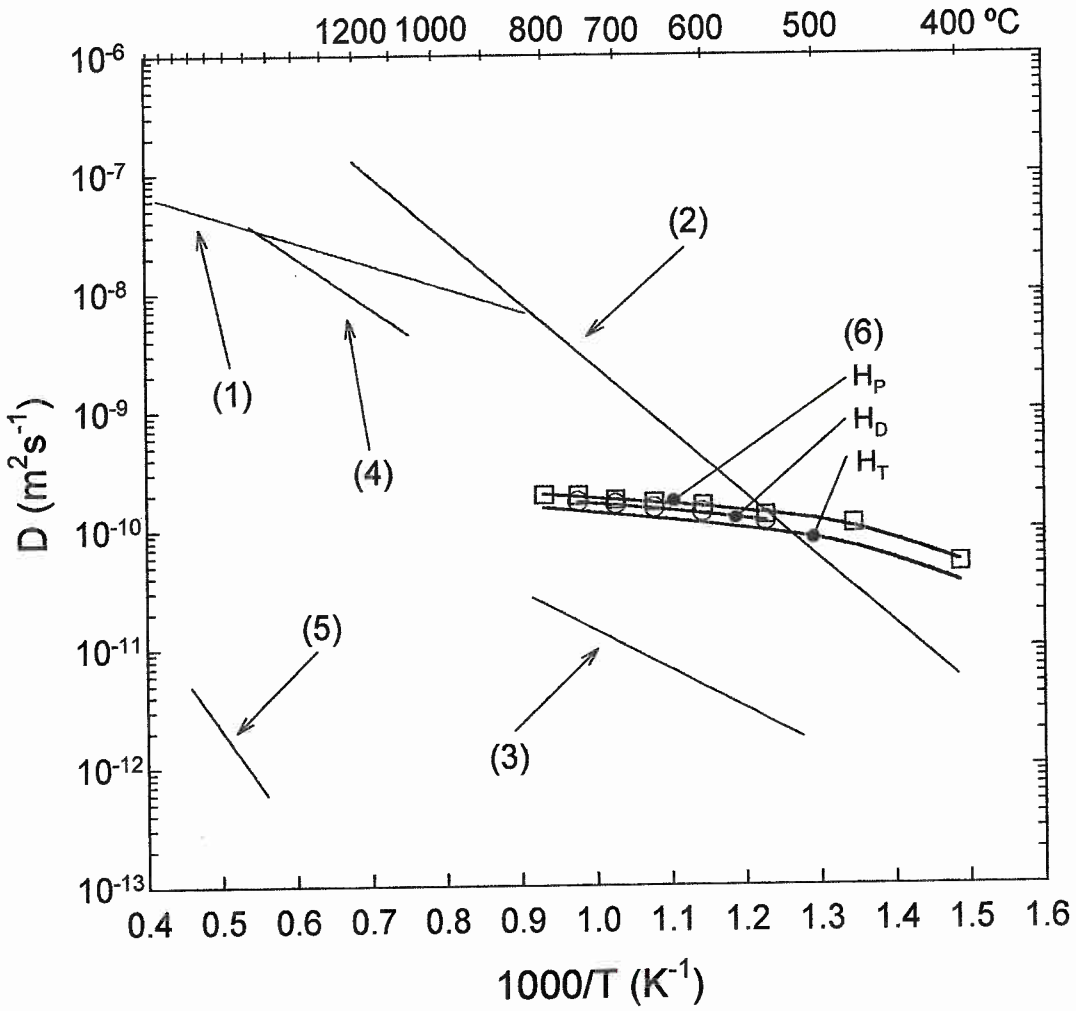

Figure 22. Hydrogen diffusivity in tungsten: (1) Frauenfelder [3], (2) Zakharov et.al. [6], (3) Kizu et.al. [4], (4) Ryabchikov [7], (5) Moore & Unterwald [5], (6) This work.

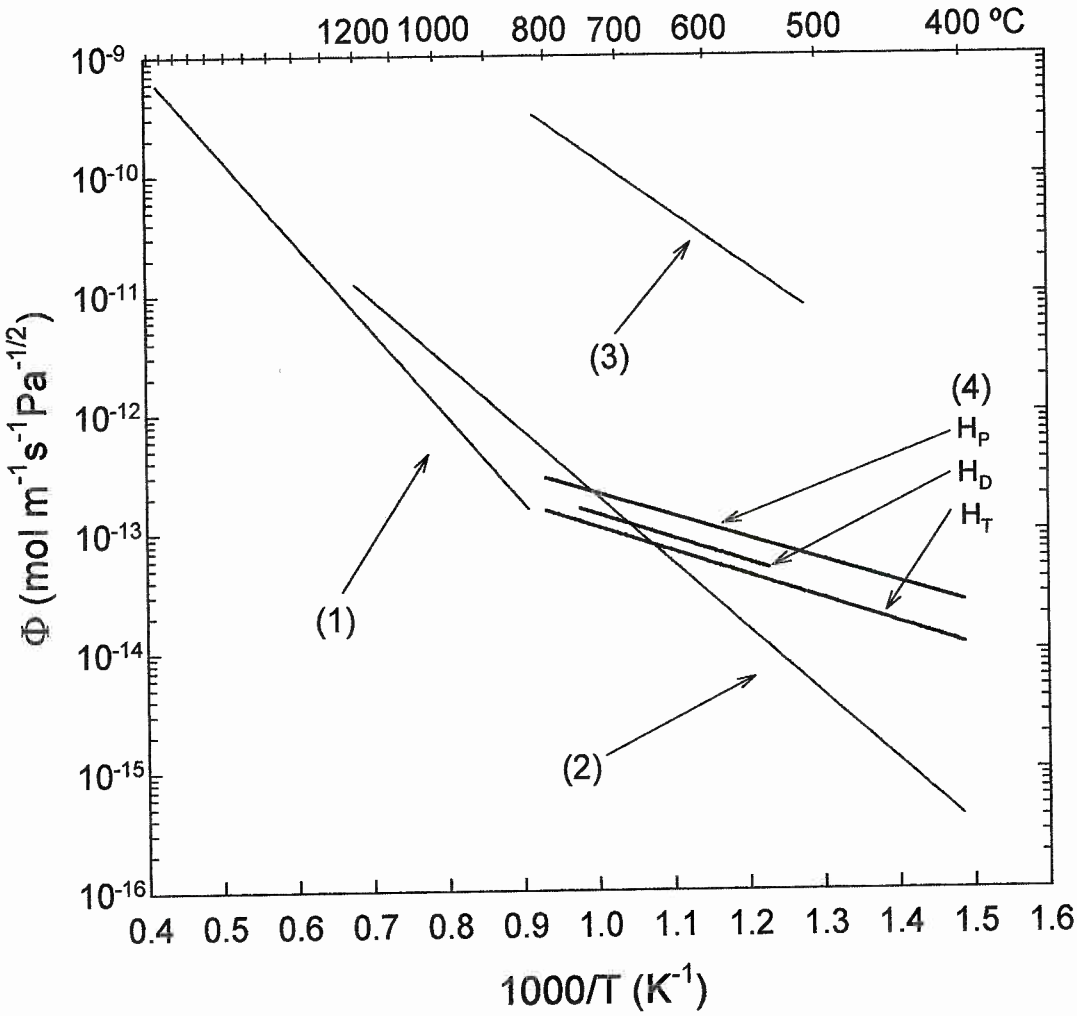

Figure 23. Hydrogen permeability in tungsten: (1) Frauenfelder [3], (2) Zakharov et.al. [6], (3) Kizu et.al. [4], (4) This work.

6. CONCLUSIONS

The isovolumetric desorption technique has been undertaken in polycrystalline tungsten, a suitable candidate to be used as plasma facing material to be employed in high heat flux components of a future thermonuclear reactor. This gas evolution method has been accomplished with H_P and H_D over a wide range of temperatures, from 673 K to 1073 K, with driving pressures from $1.3 \cdot 10^4$ to 10^5 Pa.

The H transport parameters diffusivity, solubility and permeability for H_P and H_D have been experimentally obtained; whereas the H_T values are extrapolated by means of a quantum-statistical harmonic vibration theory. A net reduction in both Sieverts' constant and diffusivity has been noticed as the mass of the isotope increased.

The trapping phenomenon has been noticed below 873 K; the characteristic trapping parameters, the number of trap sites N_t (sites/m^3) and the average trapping activation energy E_t (J/mol), are evaluated. The possibility of H clusters nucleation at structural defects has been identified as the most probable phenomenon to explain the high trapping energies obtained.

Further investigation is being undertaken with polycrystalline tungsten membranes by means of permeation technique in order to characterise the surface adsorption and recombination reactions.

7. REFERENCES

[1] G. Janeschitz, K. Borrass, G. Federici, Y. Igitkhanov, A. Kukushkin, H.D. Pacher, G.W. Pacher, M. Sugihara, J. Nucl. Mater. 220-222 (1995) 73.

[2] J.W. Davis, V.R. Barabash, A. Makhanov, L. Plöchl, K.T. Slattery J. Nucl. Mater. 258-263 (1998) 308.

[3] J. Frauenfelder J. Vac. Sci. Technol. 6 (1968) 388.

[4] K. Kizu, T. Tanabe and K. Miyazaki, 7th Int. Conf. On Fusion Reactor Materials, Obninsk, Russia, September 1995.

[5] G.E. Moore and F. C. Unterwald, J. Chem. Phys. 40 (1964) 2639.

[6] A.P. Zakharov, V.M. Sharapov and E.I. Evko, Soviet Mater. Sci. 9 (1973) 149.

[7] L.N. Ryabchikov, UKr.Fiz. Zh., 9 (1964) 293.

[8] P. Franzen, C. García Rosales, H. Plank, V.Kh. Alimov, J. Nucl Mater. 241-243 (1997) 1082.

[9] A.A. Pisarev, A.V. Varava, S.K. Zhdanov, J. Nucl Mater. 220-222 (1995) 926.

[10] R.A. Anderl, D.F. Holland, G.R. Longhurst, R.J. Pawelko, C.L. Trybus and C.H. Sellers, Fusion Technol. 21 (1992) 745.

[11] S. Alberici, A. Perujo and J. Camposilvan, Fus. Technology 28 (1995) 1108.

[12] S. Tominetti, M. Caorlin, J. Camposilvan, A. Perujo and F. Reiter, J. Nucl. Mater. 176 & 177 (1990) 672.

[13] G.A. Esteban, L.A. Sedano, A Perujo, K. Douglas, B. Mancinelli, P.L. Ceroni in "Hydrogen transport parameters and trapping effects in the martensitic steel OPTIFER-IVb", EN EUR 18995, (1999).

[14] G.A. Esteban, L.A. Sedano, A. Perujo, K. Douglas, B. Mancinelli, P.L. Ceroni in "Isotope effects in hydrogen transport parameters in the martensitic steel OPTIFER-IVb", EN EUR 15021, (1999).

[15] L. A. Sedano, A. Perujo, Chung H. Wu, J. Nucl. Mater. 273 (1999) 285.

[16] E. Serra, A. Perujo, G. Benamati, J. Nucl. Mater. 245 (1997) 285.

[17] J. Crank in: "The mathematics of diffusion". Clarendon Press, Oxford, 1956.

[18] Y. Ebisuzaki, W.J. Kass and M. O'Keeffe, J. Chem. Phys. 46 (1967) 1373.

[19] L. Haar, A.S. Friedman in : "Ideal gas thermodynamic functions and isotope exchange functions for the diatomic hydrides, deuterides, and tritides", U.S. Department of Commerce, National bureau of standards (1961).

[20] A. Seeger, Physics Letters, 58A (1976) 137.

Mission

The primary mission of SAI is to develop and promote the use of space derived data and geo-spatial data from other sources in the service of EU policies, especially those relating to agriculture, fisheries, transport and anti-fraud. SAI also seeks to make the best use of information from space systems, to maximise the return from European investments in space and to help the Union reinforce its role in international action on the environment and sustainable development.